

**STUDY OF THE MAGNETORESISTIVE
PROPERTIES OF $(La_{1.6}Dy_{0.2}Sr_{1.2})Mn_{2-x}Ni_x/Fe_xO_7$
PEROVSKITE MANGANITES**



**M. Phil. Thesis
(Physics)**

Tapashi Rani Chanda

**Roll: 040314008 F
Session: April 2003**



**DEPARTMENT OF PHYSICS
BANGLADESH UNIVERSITY OF ENGINEERING AND TECHNOLOGY (BUET)
DHAKA -1000, BANGLADESH.**





Candidate's Declaration

It is hereby declared that this thesis or any part of it has not been submitted elsewhere for the award of any degree or diploma.

Tapashi

(Tapashi Rani Chanda)

Date: 8, August, 2007
BUET, DHAKA

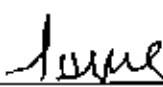
BANGLADESH UNIVERSITY OF ENGINEERING & TECHNOLOGY (BUET)
DHAKA-1000
DEPARTMENT OF PHYSICS

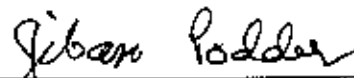


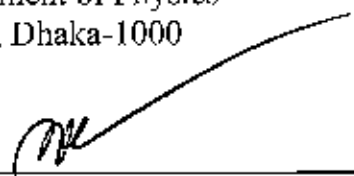
Certification of thesis work


The thesis titled "*STUDY OF THE MAGNETORESISTIVE PROPERTIES OF $(La_{1-x}Dy_{0.2}Sr_{1-x}) Mn_{2-x} Ni_x/Fe_xO_7$ PEROVSKITE MANGANITES*", submitted by TAPASHI RANI CHANDA, Roll No: 040314008F, Registration No: 0403573, Session: April 2003, has been accepted as satisfactory in partial fulfillment of the requirement for the degree of **MASTER OF PHILOSOPHY (M. Phil.)** in Physics on **8 August, 2007**.

BOARD OF EXAMINERS

1. 

Dr. Mominul Haq, (Supervisor) Chairman
Professor, Department of Physics
BUET, Dhaka-1000
2. 

Dr. Jiban Podder Member (Ex-Officio)
Professor & Head
Department of Physics
BUET, Dhaka-1000
3. 

Dr. Md. Abu Hashan Bhuiyan Member
Professor, Department of Physics
BUET, Dhaka-1000
4. 

Dr. Md. Tafazzal Hussain Member (External)
Professor, Department of Physics
University of Dhaka, Dhaka-1000

Acknowledgements

This research work has been carried out under the supervision of Professor Dr.Mominul Huq, Department of Physics Bangladesh University of Engineering and Technology (BUET), Dhaka, Bangladesh.

Firstly I must thank my supervisor Professor Dr.Mominul Huq who gave me a great opportunity to carry out this research work under his scholastic supervision. I am gladly expressing my profound sense of gratitude, sincere appreciation and indebtedness to my supervisor for his guidance, keen interest, constructive suggestions and constant inspiration throughout the research work.

I am very grateful to the Head, Dr.Jiban Podder, Professor Department of Physics Bangladesh University of Engineering and Technology (BUET), Dhaka, Bangladesh for his valuable suggestions and inspiration.

I am also very grateful to Dr.AKM Akther Hossain, Associate Professor, Department of Physics Bangladesh University of Engineering and Technology (BUET), Dhaka, Bangladesh, for his inspiration, kind co-operation and valuable suggestions during this work.

I would like to thank Prof. Dr.Md.Abu Hashan Bhuiyan, Prof. Dr.Nazma Zaman, Prof. Dr.Md. Feroz Alam Khan, Dr.Nazrul Islam, Afia Begum Department of Physics Bangladesh University of Engineering and Technology (BUET), Dhaka, Bangladesh. For their encouragement and help during this research work.

I express my sincere gratitude and thankfulness to Md.Abdul Basith, Lecturer Department of Physics (BUET), Dhaka, for his constant support and kind co-operation throughout this work.

My sincere thanks to all other teachers of physics Department, BUET for their encouragement and help through the work. I am also very much grateful to BUET authority for providing the financial fund for this research.

I would also convey my sincere thanks to Dr.Md.Fakhrul Islam Professor and head Department of Materials and Metallurgical Engineering (MME) to permit to use the facilities of high temperature furnace. Thanks to Mr.Yusuf Khan who helped me to perform the X-ray Diffraction studies for characterization of the samples.

I would also like to thanks the staff members of the Physics Department for their help.

My thanks are also due to my senior Nasrin, Shampa, Sumon,Shimul, Khurshed, Nazrul, Shaparan ,my friend Roman and all other M.Phil students for their kind help.

I am indebted to all my family member especially to my mother, brothers for their loving support and inspiration in all aspects throughout my whole life. At last my sincere tribute to my late father.

Tapashi Rani Chanda
Department of physics
BUET, Dhaka

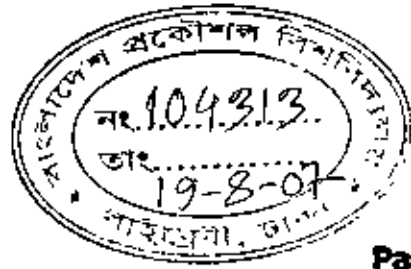
Date: 8 August, 2007

Abstract

Polycrystalline samples $(La_{1-x}Dy_xSr_{1.2})Mn_{2-x}Ni_x/Fe_xO_7$ (with $x=0.0,0.1,0.2$) were prepared using the conventional solid-state reaction technique and sintered at temperature $1100^{\circ}C$ for 24 hours in air. Phase purity and structure were checked by powder X-ray diffraction (XRD) using the MoK α radiation ($\lambda= 0.710689 \text{ \AA}$). For the structure determination, diffraction patterns were recorded in the 2θ range from 10° to 70° . The DC electrical resistivity for various polycrystalline samples was measured from room temperature down to liquid nitrogen temperature both at zero field and at applied magnetic field of 0.7T using four probe method. In the present investigation it is observed that all the samples showed metal insulator (M-I) transition with a peak in the electrical resistivity around M-I transition temperature T_p . With the increase of Ni or Fe doping the resistivity increases but M-I transition temperature T_p decreases. M-I transition temperature T_p also increased in presence of 0.7T magnetic field. Magnetoresistance (MR) measurements were carried out in a magnetic field of 0.7T in the temperature range of 77K to 300K. The MR behaviour was discussed as a function of magnetic field both at room temperature and at liquid nitrogen temperature. Room temperature MR is found to be very low, almost 0.11%–1.69% and is almost linear with field. A large value of MR is observed at 78K in the presence of low applied magnetic field. The higher percentage of Fe and Ni in these compounds enhances paramagnetic insulating phase. The plot of $\ln[\rho/\rho_0]$ vs T^{-1} curve means that the conduction occurred through a thermally activated process above the transition temperature.

Abbreviations

CMR	-Colossal magnetoresistance
GMR	-Giant magnetoresistance
MR	-Magnetoresistance
XRD	-X-ray diffraction
T_p	-Phase transition temperature
T_C	-Curie-Weiss transition temperature
T_N	-Neel temperature
$^{\circ}\text{C}$	-Degree centigrade
K	-Kelvin
eV	-Electron volt
k_B	-Boltzman constant
J_H	-Hund's exchange interaction
GB	-Grain boundary
JT	-Jahn-Teller distort
e_g	-Two-fold degenerate state (doublet state)
t_{2g}	-Three-fold degenerate state
DE	-Double exchange
FM	-Ferromagnetism
PM	-Paramagnetism
AF	-Antiferromagnetism
MI	-Metal-Insulator transition
TCR	-Temperature coefficient of resistance
CFS	-Crystal Field Splitting
TMO	-Transition Metal Oxide
HTSC	-High temperature Superconductor
LFMR	-Low Field Magnetoresistance



Contents

	Page
Chapter-1 Introduction	1
Chapter-2 Literature review	9
2.1 Emergence of a new type of magnetoresistance: Colossal magnetoresistance (CMR)	9
2.1.1 Giant magnetoresistance (GMR)	10
2.1.2 The phenomenon of magnetoresistance	12
2.2 History of manganites	13
2.3 Rare earth manganites	14
2.4.1. Electronic structure of manganites	15
2.4.2. Ionic view of electronic structure	17
2.4.3 Physical overview of doped manganites	19
2.4.4. Layered manganese oxide perovskites	22
2.4.5. Transport properties of CMR materials	23
2.4.6 Comparison of magnetotransport of few other polycrystalline samples	25
2.4.7: Intrinsic and extrinsic magnetoresistance	28
2.5 Classical double exchange model	35
2.5.1 Importance of classical double exchange model	36
2.5.2 Drawbacks of double exchange models and subsequent theories	37
2.5.3 Jahn – Teller distortion	37
2.5.4 Phase diagram and resistivity	40
2.6 Models of manganites	41
2.7 Magnetic-based device	42
Chapter-3 Sample preparation and characterization	52
3.1 Preparation of the samples	52

3.1.1 Solid state reaction method	52
3.1.2. Solution method	52
3.1.3 Melt-quenched or glass ceramic method	53
3.1.4 Thin film method	53
3.2.1. Material synthesis and sample preparation	54
3.2.2. Physicals properties	54
3.2.3. Preparation of the present samples	54
3.2.4. Methodology	55
3.3. Lattice planes and Bragg's law	55
3.4. The van der Pauw method	56
3.5 Apparatus used for the present investigation	58
3.5.1 Description of liquid nitrogen cryostat	58
3.5.2 Description of electromagnet	60
3.5.3 Description of the sample rod	61
3.5.4 Magneto resistance measurement setup	62
Chapter-4 Results and Discussion	64
4.1 X-ray diffraction analysis	64
4.2 DC electrical resistivity	66
4.3 Magnetoresistance of various polycrystalline samples	72
4.4 Activation energy	75
Chapter-5 Conclusions	79

List of Figure

Figure No	Page
Figure 2.1: Crystal structures of the most important oxides: (a) perovskite structure ($\text{La}_{0.7}\text{Ca}_{0.3}\text{MnO}_3$); (b) The MnO_2 plane, which is identical in the structure to the CuO_2 planes of the high temperature superconductors (HTSC's). (c) $n=2$ Ruddlesden–Popper phase ($\text{La}_{1.2}\text{Ca}_{1.8}\text{Mn}_2\text{O}_7$, MnO_6 octahedra are shaded, La/Ca ions are drawn as spheres).	16
Figure 2.2: Electron states of the outermost $3d$ energy level of the Mn^{3+} and Mn^{4+} ions.	17
Figure 2.3: Schematic $T=0$ density of states for doped LaMnO_3 . The level diagram to the left shows the approximate positions of the $3d$ bands in undoped LaMnO_3 . The energy scale for $\text{La}_{2/3}\text{Sr}_{1/3}\text{MnO}_3$ is extracted from photoemission data. Comparison is made to Ni metal which possesses a much smaller degree of spin polarization.	19
Figure 2.4: Resistivity against Temperature for $\text{La}_{1-x}\text{Sr}_x\text{MnO}_3$ for various x values. The arrows denote the transition as determined by magnetization measurement.	21
Figure 2.5: Top frame- magnetization against temperature for $\text{La}_{0.75}\text{Ca}_{0.25}\text{MnO}_3$ for various field values. Middle frame resistivity against temperature. The inset shows the low temperature resistivity compared to $T^{2.5}$ (solid line) and $T^{4.5}$ (dashed line) behaviour. Bottom frame- magnetoresistance against temperature. Open symbols reflect low-field behaviour and solid symbols reflect the high field behaviour.	22
Figure 2.6: The crystal structure of the layered and cubic manganites.	23
Figure 2.7: Resistivity and magnetization as a function of temperature.	24
Figure 2.8: Top panel: zero-field resistivity of $\text{La}_{0.67}\text{Sr}_{0.33}\text{MnO}_3$ single crystal and polycrystals as a function of temperature. Bottom panel: magnetization of the samples as a function of temperature measured at $B=0.5$ T. The inset shows the field-dependent magnetization at 5 and 280 K (reproduced from Hwang et al. [50]).	26
Figure 2.9: Magnetoresistance data of the samples of figure 13. Panels (a), (c) and (e): normalized resistivity ρ/ρ_0 as a function of magnetic field. ρ_0 denotes the zero-field resistivity. Panels (b), (d) and (f): magnetic field dependence of the normalized magnetization (reproduced from Hwang et al. [50]).	27

Figure 2.10: Resistivity of single-crystalline thin-film $\text{La}_{0.7}\text{Ca}_{0.3}\text{MnO}_3$ in zero magnetic field and in an applied field of 5T. The graph shows also the corresponding magnetoresistance. Adopted from Hundly et al.[53]. 29

Figure 2.11: Magnetoresistance for a field change of 0 to 2T versus temperature of polycrystalline (top panel) and epitaxial (bottom panel) thin film $\text{La}_{0.67}\text{Ca}_{0.33}\text{MnO}_3$. b) magnetoresistance as a function of applied field taken at 25 and 100K. 33

Figure 2.12: Schematic illustration of grain-boundary transport in a polycrystalline mixed-valence manganite. 34

Figure 2.13: The splitting of the t_{2g} and e_g band in $\text{La}_{1-x}\text{A}_x\text{MnO}_3$. 35

Figure 2.14: Temperature dependences of resistivity under zero magnetic field (solid lines and under 7T dotted lines for $\text{La}_{0.7}\text{Ca}_{0.3}\text{MnO}_3$, $\text{La}_{0.67}(\text{Ca,Pb})_{0.33}\text{MnO}_3$ and $\text{La}_{0.7}\text{Sr}_{0.3}\text{MnO}_3$. 36

Figure 2.15: Q_2 and Q_3 are the two Jahn – Teller modes of distortion of the oxygen octahedral associated to the splitting of the e_g levels of Mn^{3+} . These particular cases correspond to $Q_2 > 0$ and $Q_3 > 0$ is the breathing distortion that occurs due to the different sizes of Mn^{4+} and Mn^{3+} . 39

Figure 2.16: Phase diagram of temperature versus tolerance factor for $\text{A}_{0.7}\text{A}'_{0.3}\text{MnO}_3$, where A is a trivalent ion and A' a divalent ion. Open symbols denote T_C determined by magnetization measurements and closed symbols denote T_C determined by resistivity measurements. All data were taken while warming. 40

Figure 2.17: Optical response of a film of LCMO (closed circles) in comparison with the TCR (open circles). The curve is shown in the inset. 44

Figure 3.1: Bragg's law of diffraction. (a) Different forms of lattice planes, (b) Different forms atoms. 55

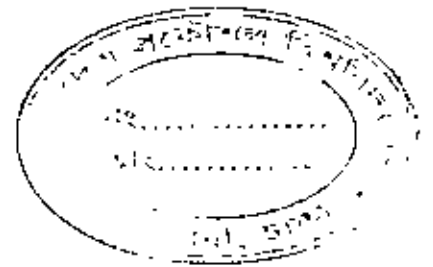
Figure 3.2: The four electrical contacts on the circumference of the discs shaped samples. 56

Figure 3.3: The function $f(Q)$ for determining the resistivity of the sample. 58

Figure 3.4: Schematic diagram of the liquid nitrogen cryostat.	59
Figure 3.5: Photograph of the electromagnet.	60
Figure 3.6: Calibration curve of the electromagnet.	61
Figure 3.7: Schematic diagram of the sample rod.	62
Figure 3.8: Schematic diagram of magnet and cryostat assembly for magnetoresistance measurements.	62
Figure 4.1: X-ray diffraction patterns of polycrystalline bulk samples.	65
Figure 4.2: Normalized resistivity as a function of temperature for $(La_{1-x}Dy_xSr_{1.2})(Mn_{2-x}Fe_x)O_7$ with $x=0.0, 0.1$ and 0.2 at 0 T magnetic field.	67
Figure 4.3: Normalized resistivity as a function of temperature for $(La_{1-x}Dy_xSr_{1.2})(Mn_{2-x}Fe_x)O_7$ with $x= 0.0, 0.1$ and 0.2 at 0.7 T magnetic field.	67
Figure 4.4: Normalized resistivity as a function of temperature for $(La_{1-x}Dy_xSr_{1.2})(Mn_{2-x}Ni_x)O_7$ with $x= 0.0, 0.1$ and 0.2 at 0 T magnetic field.	71
Figure 4.5: Normalized resistivity as a function of temperature for $(La_{1-x}Dy_xSr_{1.2})(Mn_{2-x}Ni_x)O_7$ with $x= 0.0, 0.1$ and 0.2 at 0.7 T magnetic field.	71
Figure 4.6: Magnetoresistance (MR) as a function of magnetic field at room temperature for various polycrystalline samples.	73
Figure 4.7: Magnetoresistance (MR) as a function of magnetic field at 78 K temperature for various polycrystalline samples $(La_{1-x}Dy_xSr_{1.2})(Mn_{2-x}Fe_x)O_7$ and $(La_{1-x}Dy_xSr_{1.2})(Mn_{2-x}Ni_x)O_7$ with $x= 0.0, 0.1$ and 0.2 .	74
Figure 4.8: Schematic illustration of domain-boundary transport in a polycrystalline mixed-valence manganite.	75
Figure 4.9: $\ln(\rho/\rho_0)$ is plotted against $1/T$ for various polycrystalline samples.	77

List of table

Table 4.1:	X-ray diffraction peak positions for various polycrystalline samples	66
Table 4.2:	Transition temperatures, T_p and normalized resistivity at the magnetic field 0T and 0.7T	72
Table 4.3:	Table for H^* , MR at H^* and maximum MR at 78K for various polycrystalline materials	74
Table 4.4:	Activation energy (meV) of the polycrystalline samples	76



Chapter-1

Introduction

This thesis deals with the study of the magnetoresistive properties in double-layered perovskites $(La_{1-x}Dy_{0.2}Sr_{1.2})Mn_{2-x}Ni_x/Fe_xO_7$ (with $x=0.0, 0.1, 0.2$). Like prototype materials $R_{1-x}A_xMnO_3$ where R is a trivalent rare-earth cation (e.g La, Pr, Nd, Gd, Sm, Ho etc) and A is a divalent cation (like Ba, Ca, Sr etc).

A tremendous interest has grown in magnetotransport phenomena in magnetic oxides in recent years. Studies were stimulated by the discovery of colossal magnetoresistance (CMR) in ferromagnetic perovskite of the type $La_{1-x}Sr_xMnO_3$ [1]. The manganites display a rich phase diagram [2] as a function of temperature, magnetic field and doping that is due to the intricate interplay of charge, spin, orbital and lattice degrees of freedom. Recently, the Ruddlesden-Popper $(La_{1-x}Sr_x)_{n+1}Mn_nO_{3n+1}$ perovskites based mixed valence layered manganites [3,4] also have been the subject of intense research efforts. Potential applications of the CMR effect in mixed-valence manganites include magnetic sensors; magnetoresistive read heads, and magnetoresistive random access memory. After the discovery of CMR in some manganites materials [5,6], enormous number of experimental and theoretical studies have been carried out in order to understand the CMR phenomenon and furthermore to explore this unique property for potential applications. But till now CMR is found on a magnetic field scale of several tesla and at a very low temperature, which is not very appealing for applications.

Double exchange [7-11] has been featured prominently in the discussion of the fascinating properties of the CMR materials. Within the double-exchange model it is assumed that the presence of Mn^{4+} due to the doping, enables the e_g electron of a Mn^{3+} ion to hop to the neighboring Mn^{4+} ion which ultimately mediates ferromagnetism and conduction. To date, much of the exploration of the CMR materials has been done through doping of the La sites, which brings about lattice effects, and ultimately influence the double exchange. However, very few studies have been conducted in doping the Mn sites, which are at the heart of the double exchange.

Recently, the double-layered manganites of nominal composition $\text{La}_{2-2x}\text{Sr}_{1+2x}\text{Mn}_2\text{O}_7$ has become of special interest since they show an extremely rich variety of magnetic structure as a function of doping and since they allow for the study of dimensionality effects on the electronic and magnetic properties in the doped CMR manganites. Large MR has been observed for $\text{La}_{2-2x}\text{Sr}_{1+2x}\text{Mn}_2\text{O}_7$ [12]. It was found that the layered manganites structure such as single crystals of $\text{La}_{1.8}\text{Sr}_{1.2}\text{Mn}_2\text{O}_7$ and $\text{La}_{1.2}\text{Sr}_{1.8}\text{Mn}_2\text{O}_7$ [12] also leads to an enhanced low field CMR effect. In these cases, the magnetic coupling between t_{2g} local spins in the MnO_2 bilayers is at least an order of magnitude stronger than that of interbilayers. The layered manganites $\text{La}_{2-2x}\text{Sr}_{1+2x}\text{Mn}_2\text{O}_7$ are the $n=2$ member of the Ruddiesden-Popper series $(\text{La}_{1-x}\text{A}_x)_{n+1}\text{Mn}_n\text{O}_{3n+1}$ which can be thought of as perovskite blocks of n layers separated by a rock-salt $(\text{LaA})_2\text{O}_2$ layer which decouples the blocks electrically and magnetically[13].

Asano et. al. [14] measured giant magnetoresistance of a two-dimensional ferromagnet $\text{La}_{2-2x}\text{Ca}_{1+2x}\text{Mn}_2\text{O}_7$ have been successfully synthesized and investigated with respect to their magnetic and electrical properties. It was found that $\text{La}_{2-2x}\text{Ca}_{1+2x}\text{Mn}_2\text{O}_7$ ($x=0.25$) is a metallic ferromagnet with a magnetic transition temperature T_c of 215 K.

Dorr et. al. [15] measured magnetoresistance of polycrystalline $\text{La}_{2-2x}\text{Sr}_{1+2x}\text{Mn}_2\text{O}_7$ mixed valent ($\text{Mn}^{3+}/\text{Mn}^{4+}$) manganites. Temperature and field dependence of magnetization and of electrical resistivity have been measured between 5 K and room temperature. From room temperature down to metal-insulator transition temperature, thermally activated behavior was found for both samples. The metal-insulator transition temperature roughly coincides with the curie temperature obtained from magnetization measurements. The $x = 0.5$ compound orders antiferromagnetically near $T_N = 215\text{K}$, showing a resistivity enhancement there. The resistivity of the $x = 0.4$ compound shows a field dependence at low temperature similar to that found for polycrystalline $\text{La}_{0.7}\text{Sr}_{0.3}\text{MnO}_3$.

Philip. et. al. [16] investigates microstructure and magnetoresistance of epitaxial films of the layered perovskite $\text{La}_{2-2x}\text{Sr}_{1+2x}\text{Mn}_2\text{O}_7$ ($x = 0.3$ and 0.4) by laser molecular beam epitaxy on NdGaO_3 and SrTiO_3 substrates. For $x = 0.4$, both the ab -or in-plane resistivity ρ_{ab} as well as the c -axis or out-of-plane resistivity ρ_c qualitatively show a ferromagnetic

metal (*FM*) to paramagnetic insulator (*PI*) transition around 120 K [12,17]. For $x=0.3$, two separate magnetic transitions occur at 270 K and 90 K which have been attributed to the presence of 2D and 3D magnetic correlations, respectively [18]. Philip. et. al found that a comparison of magnetotransport measurements within the *ab* plane and along the *c*-axis direction showed an intrinsic *c*-axis tunneling magnetoresistance effect associated with non-linear current-voltage characteristics for the $x=0.3$ compound.

Shimakawa et. al.[19] in their investigation measured giant magnetoresistance in $Tl_2 Mn_2 O_7$ with the pyrochlore structure and found that near T_c the applied magnetic field tends to align the local spins, and then electron transfer increases. As a result a sharp resistivity decrease is observed. Powder samples of $Tl_2 Mn_2 O_7$ (~500 mg) were synthesized by solid-state reaction method, Shimakawa et. al found that Mn 3d orbitals are split into t_{2g} and e_g states by the crystal field. Although both perovskite and pyrochlore manganese oxide structure consists of MnO_6 octahedra with vertex sharing, these structures have different networks. In a pyrochlore structure, the MnO_8 or Mn_2O_6 with a Mn-O-Mn bond angle of $\sim 130^\circ$ In a perovskite structure, in contrast, has a simple cubic network of MnO_6 with a nearly 180° bond angle.

In the measurements of Asano et. al, [14], Dorr et al.[15], Philipp et. al.[16] and Basith et. al.[20] the exhibited electric and magnetic transport properties were described either by traditional double exchange mechanism based on the mixed Mn^{3+}/Mn^{4+} valence state or by dynamic Jahn-Teller lattice distortion due to different atomic sizes of the cations.

Most recently, huge experimental work [21-24] is being performed again on the rare earth manganites of the type $R_{1-x}A_xMnO_3$ or $R_{1-x}A_xMn_yF_yO_3$ ($F=Fe, Co, Ni, Cr$) to investigate the transport properties like electron-electron, electron-phonon, electron-magnon scattering process in the low temperature metallic phase ($T < T_p$) and the nature of hopping conduction in the high temperature insulating phase ($T > T_p$). In spite of enormous experimental research work on prototype materials [24-28], the conduction mechanism of *CMR* materials below and above T_p is not well understood. On the contrary, this kind of research is quite inadequate in bilayered perovskites $R_{2-2x}A_{1+2x}Mn_2O_7$.

In the present work, the Fe and Ni doped $(La_{1.6}Dy_{0.2}Sr_{1.2})Mn_{2-x}Ni_x / Fe_xO_7$ ($x=0.0, 0.1, 0.2$) perovskite was prepared to investigate the electrical transport and magnetoresistive properties from room temperature down to liquid nitrogen temperature. It is found that all samples display an *M-I* transition depending on Mn content, thus temperature dependence resistivity data was analyzed to know the scattering process below *M-I* transition temperature and the hopping conduction above *M-I* transition temperature.

The magnetic moment of Fe and Ni is $2.12 \mu_B$ and $0.62 \mu_B$ respectively, whereas the magnetic moment of Mn^{3+} and Mn^{4+} is $4 \mu_B$ and $3 \mu_B$ respectively. Previous studies showed that the ferromagnetic to paramagnetic transition temperature (T_p) of layered manganites like $La_{2-2x}Sr_{1+2x}Mn_2O_7$ ($x=0.3-0.4$) is around 125K [29] but the ferromagnetic transition temperature of Fe and Ni is 1043 K and 627 K, respectively. The same ionic radii of Fe^{3+} and Mn^{3+} may not cause any structural change but may suppress strongly the charge ordering. So when Mn ions are replaced with Fe and Ni, the magnetoresistive properties, ferromagnetic metal to paramagnetic insulator transition temperature of the investigated compound would change due to the change in the size of the ions, change in magnetic moments, high curie temperature and also due to the strengthening or weakening of the double exchange interaction between two unlike ions. In the present investigation, the results of an experimental study of the doping of the Mn sites by ferromagnetic Fe and Ni in $(La_{1.6}Dy_{0.2}Sr_{1.2})(Mn_{2-x}Fe_x)O_7$ and $(La_{1.6}Dy_{0.2}Sr_{1.2})(Mn_{2-x}Ni_x)O_7$ with $x=0.0, 0.1, 0.2$ in respect of their magnetoresistance as a function of magnetic field both at room temperature (RT) and liquid nitrogen temperature, resistivity as a function of temperature (RT to 78K) both at zero field and at an applied magnetic field of 0.7T and thermal activation energy and variable- range hopping behavior in the paramagnetic state have been investigated.

Objectives of the present study

* To study the effect of substitution of Mn by Ni/Fe in electrical transport and magnetoresistive behavior of polycrystalline $(La_{1.6}Dy_{0.2}Sr_{1.2})Mn_{2x}Ni_x/Fe_xO_7$ ($x=0.0, 0.1, 0.2$).

- * To improve the value of transition temperature.
- * To understand the mechanism of CMR properties in these materials.

Sketch of the contents

In this dissertation the preparation, characterization and magnetoresistive properties of the polycrystalline sample $(\text{La}_{1.6}\text{Dy}_{0.2}\text{Sr}_{1.2})\text{Mn}_{2-x}\text{Ni}_x/\text{Fe}_x\text{O}_7$ ($x = 0.0, 0.1, 0.2$) is described.

Chapter 2 Gives a brief description of the existing theories and mechanisms of CMR manganites.

Chapter 3 Describes the details of the sample preparation and experimental techniques used in the present investigation.

Chapter 4 Presents results on magnetoresistive properties of polycrystalline sample $(\text{La}_{1.6}\text{Dy}_{0.2}\text{Sr}_{1.2})\text{Mn}_{2-x}\text{Ni}_x/\text{Fe}_x\text{O}_7$ ($x = 0.0, 0.1, 0.2$)

Chapter 5 Summarizes the findings of this dissertation.

References

- [1] von Helmolt R., Wecker J., Holzäpfel B., Schütz L., and Samwer K., "Giant negative magnetoresistance in Perovskite $\text{La}_{2/3}\text{Ba}_{1/3}\text{MnO}_x$ ferromagnetic films", *Phys. Rev. Lett.* **71**,2331. (1993).
- [2] Schiffer P., Ramirez A.P., Bao W. and Cheong S-W., "Low temperature magnetoresistance and the magnetic phase diagram of $\text{La}_{1-x}\text{Ca}_x\text{MnO}_3$ ", *Phys. Rev. Lett.* **75**, 3336. (1995).
- [3] Asano H., Hayakawa J. Matsui M., 'Giant magnetoresistance of a two-dimensional ferromagnet $\text{La}_{2-2x}\text{Ca}_{1+2x}\text{Mn}_2\text{O}_7$ ', *Appl. Phys. Lett.*, **68**,3638. (1996).
- [4] Welp U., Berger A., Vlasko-Vlasov V.K., Li Q., Gray K.E., and Mitchell J.F., 'Magnetic anisotropy and domain structure of the layered manganite $\text{La}_{1.36}\text{Sr}_{1.64}\text{Mn}_2\text{O}_7$ ' *Phys. Rev. B* **62**,8615.(2000).
- [5] von Helmolt R., Wecker J., Haupt L, and Barner K., 'Intrinsic giant magnetoresistance of mixed valence La-A-Mn oxide (A=Ca, Sr,Ba)', *Journal of Applied Physics*, **76** (10),6925. (2000)
- [6] Coey, J.M.D., Viret M., and von Molnar S., 'Mixed-valence manganites' *Advances in physics*, **48**(2),167. (1999).
- [7] Zener C., 'Interaction between the s-shells in the transition metals: ferromagnetic compounds of manganese with perovskite structure', *Phys. Rev.* **82** 403. (1951).
- [8] Anderson P.W. and Hasergewa H., 'Considerations on double exchange', *Phys. Rev.***100** 675. (1951).
- [9] de Gennes P-G., 'Effects of double exchange in magnetic crystals' *Phys. Rev.***118** 141. (1990).
- [10] Searle C. W. and Wang S.T., 'Studies of the ionic ferromagnet $(\text{La,Pb})\text{MnO}_3$, V. Electric transport and ferromagnetic properties' *Can. J. Phys.* **48** 2023.
- [11] Kubo K. and Ohata N. 'A quantum theory of double exchange', *J. Phys. Soc. Japan* **33** 21. (1972)
- [12] Moritomo Y., Asamitsu A., Kuwahara H., and Takura, Y. "Giant magnetoresistance manganese oxides with a layered perovskite structure", *Nature*, (London) **380**, 141 (1996).
- [13] Rnddlesdon S.N. and Popper P., *Acta, Cryst.* **11**, 541 (1958).

- [14] Asano H., Hayakawa J., and Matsui M., "Magnetoresistance in thin films and bulks of layered-perovskite $\text{La}_{2-2x}\text{Ca}_{1+2x}\text{Mn}_2\text{O}_7$ ", *Appl. Phys. Lett.* **70**, 2303 (1997).
- [15] Dorr K., Muller K.-H., Ruck K., Krabbes G., and Schultz L., "Magnetoresistance of polycrystalline layered manganites $\text{La}_{2-2x}\text{Sr}_{1+2x}\text{Mn}_2\text{O}_7$ ", *J. Appl. Phys.* **85**, 5420 (1999).
- [16] Philipp J.B., Klein J., Recher C., Walther T., Mader W., Schmid M., Suryanarayanan R., Alff L., and Gross R., "Microstructure and magnetoresistance of epitaxial films of the layered perovskite $\text{La}_{2-2x}\text{Sr}_{1+2x}\text{Mn}_2\text{O}_7$ ($x=0.3$ and 0.4)", *Phys. Rev. B* **65** 18441 (2002).
- [17] Imada M., Fujimori A., and Tokura Y., *Rev. Mod. Phys.* **70**, 1039 (1998).
- [18] Kimura T., Tomioka Y., Kuwahara H., Asamitsu A., Tamura M., and Tokura Y., *Science* **274**, 1698 (1996).
- [19] Shimakawa Y., Kubo Y., and Monako T., "Giant magnetoresistance in $\text{Tl}_2\text{Mn}_2\text{O}_7$ with the pyrochlore structure", *Nature (Japan)* **379**, 53-55 (1996).
- [20] Basith M.A., and HUQ M., "Magnetoresistive properties of Gd Doped Lanthanum Strontium Manganites", *Journal of Ultra Chemistry*, Vol. 1, NO. 2, 29-36, 2005.
- [21] Jiyu Fan Li, Pi Sicheng Liao, Yuheng Zhang, *Journal of magnetism and magnetic materials* (article in press). Available online at www.sciencedirect.com.
- [22] Sudipta Pal, Esa Bose, B.K. Chaudhuri, H.D. Yang, S. Neeleshwar, Y. Y. Chen, "Effect of Ni doping in rare-earth manganite $\text{La}_{0.7}\text{Pb}_{0.3}\text{Mn}_{1-x}\text{Ni}_x\text{O}_3$ ($x=0.0-0.5$)", *Journal of magnetism and magnetic materials*, **293**, 872 (2005).
- [23] Arita Banerjee, S. Pal, and B.K. Chaudhuri, "Nature of small-polaron hopping conduction and the effect of Cr doping on the transport properties of rare-earth manganite $\text{La}_{0.5}\text{Pb}_{0.5}\text{Mn}_{1-x}\text{Cr}_x\text{O}_3$ ", *Journal of Chemical Physics*, **115**, 1550 (2001).
- [24] Li Pi, Lei Zheng, and Yuheng Zhang, "Transport mechanism in polycrystalline $\text{La}_{0.825}\text{Sr}_{0.175}\text{Mn}_{1-x}\text{Cu}_x\text{O}_3$ ", *Phys. Rev. B*, **61**, 8917 (2000).

- [25] Jeffrey Snyder G., Hiskes R., Dicarolis S., Beasley M. R., and Geballe T. H., "Intrinsic electrical transport and magnetic properties of $\text{La}_{0.67}\text{Ca}_{0.33}\text{MnO}_3$ and $\text{La}_{0.67}\text{Sr}_{0.33}\text{MnO}_3$ MOCVD thin films and bulk material", *Phys. Rev. B* **53**, 14434 (1996).
- [26] Teresa De J. M., Ibarra M. R., Blasco J., Garcia J, Marquina C., and Algarabel P.A., "Spontaneous behavior and magnetic field and pressure effects on $\text{La}_{2/3}\text{Ca}_{1/3}\text{MnO}_3$ perovskite", *Phys. Rev. B* **54**, 1187 (1996).
- [27] Urushibara A., Moritomo Y., Arima T., Asamitsu A, Kido G., Tokura Y, "Insulator-metal transition and giant magnetoresistance in $\text{La}_{1-x}\text{Sr}_x\text{MnO}_3$ ", *Phys. Rev. B* **51**, 14103, (1995).
- [28] Schiffer P., Ramirez, A.P. Bao W., and Cheong S. W., "Low temperature magnetoresistance and the magnetic phase diagram of $\text{La}_{1-x}\text{Ca}_x\text{MnO}_3$ ", *Phys. Rev. Lett.* **75**, 3336, (1995)
- [29] Philipp J.B., Klein J , Recher C, Walther T, Mader W, Schmid M, Suryanarayanan L. Alff and R Gross, (2002), "Microstructure and Magnetoresistance of epitaxial films of the layered perovskites $\text{La}_{2-2x}\text{Sr}_{1+2x}\text{Mn}_2\text{O}_7$ ($x=0.$ and 0.4)", *Phys. Rev. B*, **65** 184411.

Chapter-2

Literature review

In this chapter, brief descriptions of the basic issues of colossal magnetoresistance (CMR) in manganites are given. Theoretical explanations of CMR materials including the electronic structure of the manganites are described briefly. The bulk magnetic and transport properties of manganites and various phase diagrams as a function of doping, temperature, external magnetic field and hydrostatic pressure etc. are also presented here. Various models such as double exchange theory, Jahn – Teller effects, variable range hopping in manganites, electron correlation effects are discussed briefly. Various models of low temperature magnetoresistance and grain boundary magnetoresistance in the doped manganites are also discussed here.

2.1 Emergence of a new type of magnetoresistance: Colossal magnetoresistance (CMR)

Another magnetoresistive material which has drawn considerable attention in the last decade are the unique intrinsically layered perovskite (ABO_3 type) manganites of the form $RE_{1-x}AE_xMnO_3$, where RE is a trivalent rare earth element e.g La, Pr, Nd, etc. and AE is divalent alkaline earth element e.g. Ca, Ba, Sr, etc. Chahara et. al.(1993) [1], von Helmholtz et. al.(1993) [2] and Jin et. al.(1994) [3] observed a high magnetoresistance in these doped rare earth manganites (bulk as well as thin films) in a magnetic field of several tesla ($\sim 6T$).

As the physical origin of the magnetoresistance in manganites was completely different from the Giant magnetoresistance effect (GMR), and hence the term colossal was coined [3] to describe the effect. The initial interest in the potential applications of colossal magnetoresistance was soon prompted by the complexity of the materials. In these materials, the interaction between the electrons and lattice vibrations (phonons) is usually strong, leading to a wide range of striking physical phenomena and most crucially, can be

tuned over a wide range by variation of chemical composition, temperature and magnetic field[2]. These materials therefore provide an unprecedented opportunity to study the poorly understood physics of systems in which a high density of electrons is strongly coupled to phonons that demand a microscopic and ultimately atomic characterization of structure, electronic structure and dynamics. The relationships between these structural, electronic, magnetic and optical properties are to be explained in a systematic way.

The research has given rise to important physical concepts, such as double exchange mechanism and the Jahn-Teller polaron, optically and electrically induced magnetic phase transitions, colossal intrinsic magnetoresistance and grain boundary magnetoresistance. The rich electronic phase diagrams reflect the balance of interaction, which together determine the electronic ground state. Their properties have been studied for years, both theoretically and experimentally, but a complete understanding remains elusive.

2.1.1. Giant magnetoresistance (GMR)

The Giant magnetoresistance (GMR) was discovered in 1988 independently by Baibich et al.[4] in Paris and Binasch et. al [5] in Julich. It is the phenomenon where the resistance of certain materials drops dramatically as a magnetic field is applied. It is described as Giant since it is a much larger effect than had ever been previously seen in metals. It has generated interest from both physicists and device engineers, as there is both new physics to be investigated and huge technological applications in magnetic recording and sensors.

The GMR effect is most usually seen in magnetic multilayered structures, where two magnetic layers are closely separated by a thin spacer layer of few nm thick. It is analogous to a polarization experiment, where aligned polarizers allow light to pass through, but crossed polarizer do not. The first magnetic layer allows electrons in only one spin state to pass through easily - if the second magnetic layer is aligned then that spin channel can easily pass through the structure, and the resistance is low. If the second

magnetic layer is misaligned then both spin channels can get through the structure easily and the electrical resistance is high. The GMR effectively measures the difference in angle between the two magnetizations in the magnetic layers. Small angles (parallel alignment) gives a low resistance, large angles (anti parallel alignment) gives a higher resistance. It is easy to produce the state where the two magnetic layers are parallel simply apply a field large enough to magnetically saturate both layers.

The GMR effect was originally discovered in molecular beam epitaxy grown epitaxial (100) oriented Fe/Cr/Fe sandwiches [18] and Fe/Cr multilayer [4] but the effects were quite modest at room temperature. Shortly afterwards it was discovered that similar effects could be found in polycrystalline sputtered Fe/Cr multilayer and subsequently very large room temperature MR was found in Co/Cu and related multilayer [6-8]. The GMR has also been observed in a variety of inhomogeneous granular (clusters and alloys) systems predominately comprised of Fe, Co, Ni and their various alloys in Cu, Ag and Au matrices [9-11]. In granular magnetic systems, where small ferromagnetic grains (e.g. Fe, Co, Ni etc.) are embedded in an immiscible insulating matrix, the macroscopic properties depend on the metallic volume fraction 'x', the grain size and inter granular distance. When the relative orientation of grain is anti parallel, it results in a minimum in conductance. When anti parallel grains are forced to be parallel by the application of a magnetic field, conductance increases and results in large magnetoresistance [12,13]. On the other hand, in magnetic multi layers spin dependent scattering (SDS) at the interface is responsible for the GMR effect [14].

Grunberg et. al.(1986) [15] have observed MR in thin film multi layers comprising of two layers of Fe, and Cr layer sandwiched between them. The report of Gruenberg went unnoticed by most researcher till Baibich et. al.(1988) [4], independently observed a drop in resistivity of almost 50% in artificially engineered multi layers by application of external magnetic field and named the phenomenon as Giant Magnetoresistance (GMR). Parkin et.al.(1995) [16] have found that the relative orientation of the magnetic moments of two neighbouring Co (magnetic) layers depends on the thickness of the intervening spacer Cu (nonmagnetic) layer.

2.1.2 The phenomenon of magnetoresistance

Recent years magnetoresistance has been the centre of many investigations due to applications in magnetic storage and sensing device. The resistivity of some materials is greatly affected when the material is subjected to a magnetic field. This phenomenon is known as magnetoresistance.

Magnetoresistance (MR) is defined as the change in the electrical resistance produced by the application of an external magnetic field. It is usually given as a percentage. It can be percentage by the equation given below

$$MR\% = \frac{\rho(H) - \rho(0)}{\rho(0)} \times 100 \dots\dots\dots (2.1)$$

Where $\rho(H)$ is the resistivity in an applied magnetic field and $\rho(0)$ is the resistivity in the absence of a magnetic field (at zero field). With this definition, the magnetoresistance has a maximum value of 100%.

MR can be negative or positive. In non-magnetic pure materials and alloys MR is always positive and MR shows a quadratic dependence on applied magnetic field. MR can be negative in magnetic materials because of the suppression of spin disorder by the magnetic field i.e. the application of a magnetic field causes a dramatic decrease of the resistivity. Heterogeneous ferromagnetic materials such as thin film multi layers and cluster-alloy compounds display large MR referred to as giant magnetic resistance (GMR). Usually, the magnitude of the magnetic field that is necessary to get this large magnetoresistance range is in order of several tesla.

All metals show some MR, but upto only a few percent. Nonmagnetic metals such as Au, exhibit small MR, but the magnitude is somewhat greater (upto 15%) in ferromagnetic metals such as Fe and Co. The semimetal Bi also shows ~ 18% MR in a transverse field of 0.6T, which rises to a 40-fold change at 24T [17]. Cu is more typical in that the same very powerful field (24T) gave rise to change of only ~2% at room temperature. This is the classical positive magnetoresistance that varies as B^2 (B = applied magnetic field) in

half metallic ferromagnets such as CrO_2 , Fe_3O_4 at low temperature [18]. It is absent in the free electron gas [19] but appears when the Fermi surface is non-spherical. This MR originates from the impact of the Lorentz force on the moving charge carriers similar to the Hall effect. Its value is $\sim 10\%$ at 10T. A classification of magnetoresistance phenomenon is based on the distinction familiar in magnetism between intrinsic properties such as anisotropy constants, which depend only on the crystal structure, composition and purity, and extrinsic properties of manganites.

2.2 History of manganites

In 1950 Jonker and Santen [20-22] described the preparation of polycrystalline manganites sample of $(\text{La,Ca})\text{MnO}_3$, $(\text{La,Sr})\text{MnO}_3$ and $(\text{La,Ba})\text{MnO}_3$ and reported ferromagnetism and anomalies in the conductivity at the Curie temperature with variation in lattice parameter as a function of hole doping. Few years later Volger [23] observed a notable decrease of resistivity for $\text{La}_{0.8}\text{Sr}_{0.2}\text{MnO}_3$ in ferromagnetic FM state, in applied magnetic field. Soon after a significant research effort has started on the studies of low temperature measurements in magnetic, such as specific heat, magnetization, dc and ac resistivity, magnetoresistance, I-V curves, dielectric constant, Seebeck effect and Hall effect [23,24].

In 1955 Wollan and Koehler [25] carried out extensive neutron diffraction study to characterize and draw the first magnetic structures of $\text{La}_{1-x}\text{Ca}_x\text{MnO}_3$ in the entire composition range. In that time they were among the first to use the technique of neutron scattering to study magnetism in materials. They found that in addition to FM phase many other interesting antiferromagnetic phases were also present in manganites.

In 1979 Jirak et. al. [26] and in 1982 Pollert et. al. [27] studied the structure and magnetic properties of another very popular manganite $(\text{Pr,Ca})\text{MnO}_3$ by X-ray and neutron diffraction technique. They observed charge-ordering phases which are totally different from ferromagnetic phases of other manganites.

In 1990 a burst research activity on manganites started because of the observation of large magnetoresistance. In 1989 worked by Kusters [28] on bulk $\text{Nd}_{0.5}\text{Pb}_{0.5}\text{MnO}_3$ reveals the large MR effect at room temperature. In 1993 another work by von Helmholtz *et. al.* [2] on thin films of $\text{La}_{2/3}\text{Ba}_{1/3}\text{MnO}_3$ also revealed a large MR effect at room temperature. In 1993 Chahara [1] was reached the similar conclusion using thin films of $\text{La}_{3/4}\text{Ca}_{1/4}\text{MnO}_3$ and in 1994 Ju *et. al.* [29] for films of $\text{La}_{1-x}\text{Sr}_x\text{MnO}_3$. They all observed MR values for larger than those observed in artificially engineered multilayers (GMR) [16].

In 1994, Jin *et. al.* [3] reported the same that it is possible to reduce the resistivity by several orders of magnitude under the application of very large magnetic field in hole doped manganese oxide perovskites near the curie temperature T_c . The term colossal magnetoresistance (CMR) was coined to make a distinction with the GMR found earlier metallic super lattices by switching the external field [4,30,6]. GMR is caused by introducing interface in spin polarized conductors and is restricted below T_c whereas CMR is a bulk property which originates from magnetic ordering and is usually confined to the vicinity of T_c . In particular, Jin *et al.* [3] reported maximum values of around 100,000% for thin films of calcium doped manganese oxide near 77 K with an applied magnetic field of 6T. They also remarked that their results had a very strong dependence on the method used to grow the films. MR had also been observed in other manganese oxide perovskite [28], but the values reported were not so high.

2.3 Rare earth manganites

Mixed-valence manganites with the perovskite structure have been studied for almost 50 years. Early research was motivated by a need to develop insulating ferromagnetism with a large magnetization for high-frequency applications. Recent work has been driven by a desire to understand and exploit the large negative magnetoresistance effect that appears near the curie temperature.

Coccy *et.al* [54] has recently reviewed the extensive literature on the physical properties of mixed- valence manganites and there are short reviews on colossal Magnetoresistance

and theoretical aspects by Ramirez (1997) [89] and Nagaev (1996) [90] respectively. The perovskite manganites can be expressed in terms of the general formula ABO_3 , where A site is randomly La or Ca and B site is Mn.

2.4.1. Electronic structure of manganites

Mixed valence manganites, with the composition $AMn^{3+}O_3$ or $BMn^{4+}O_3$ is one family of the larger group of transition metal oxides, which includes other families such as ferromagnetic titanites. Most manganite perovskite crystals, including layered perovskites. The parent compound crystallizes in $AMnO_3$ type perovskite structure having general formulas $RE_{1-x}AE_xMnO_3$, where RE stands for trivalent rare earth cation such as La, Pr, Nd, Sm, Eu, Gd, Tb, Y etc. and AE stands for divalent alkaline earth cation such as Ca, Sr etc. In this perovskite like structure (RE,AE) occupies the vertices of the cubic unit cell, Mn occupies the body center and O occupies the six faces of the cube which forms MnO_6 octahedra [31,32,33]. Most manganite perovskite crystals, including layered perovskites. However, some manganites can be formed of hexagonal layered crystal structures which are different from the cubic structure in atomic view, play some important role resulting different physical characteristics [34].

The perovskite crystal structure can be regarded as a three dimensional network of corner sharing MnO_6 octahedra, with Mn ions in the middle of the octahedra. Eight octahedra form a cube, with the A site in its center. In the cubic perovskite, the A-site is twelve-fold surrounded by oxygen ions. But typically the ionic radius of the A ion is similar to the volume enclosed by the oxygen ions. This volume is reduced by rotating the octahedra with respect to each other. Inevitably the twelve A-O bond lengths become inequivalent.

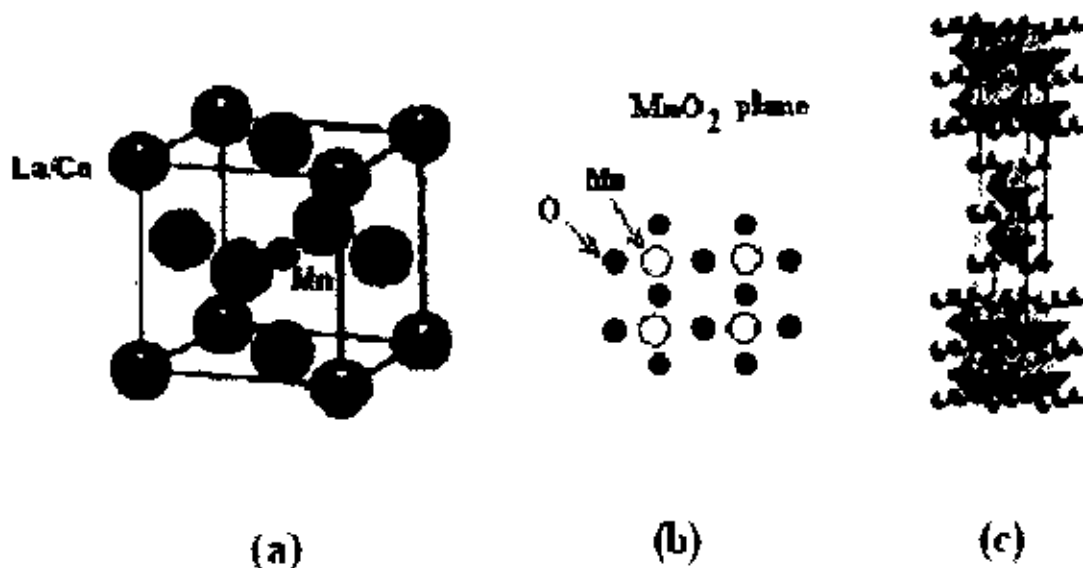


Figure 2.1: Crystal structures of the most important oxides: (a) perovskite structure ($\text{La}_{0.7}\text{Ca}_{0.3}\text{MnO}_3$); (b) The MnO_2 plane, which is identical in the structure to the CuO_2 planes of the high temperature superconductors (HTSC's). (c) $n=2$ Ruddlesden-Popper phase ($\text{La}_{1.2}\text{Ca}_{1.2}\text{Mn}_2\text{O}_7$, MnO_6 octahedra are shaded, La/Ca ions are drawn as spheres).

The perovskites crystal structure can be regarded as a three dimensional network of corner sharing MnO_6 octahedra, with Mn ions in the middle of the octahedral. Eight octahedra form a cube, with the A site in its centre. In the cubic perovskite, the A site is twelve-fold surrounded by oxygen ions. But typically the ionic radius of the A ion is smaller than the volume, enclosed by the oxygen ions. This volume can be reduced by rotating the octahedra with respect to each other. Inevitably the twelve A-O bond lengths become nonequivalent.

The first report on the crystal structure of the manganites dates back to 1943 by Naray-Szabo [35] and was revised by Yakel [36] in 1955. In contrast to the single cubic unit cell reported by Naray-Szabo, Yakel proposed a monoclinic unit cell, nearly identical to the double cubic cell, but for one angle that is slightly larger than 90° . Although the perovskites structure itself was not under discussion, the exact modification was controversial. The AMnO_3 has the $Pnma$ space group. Just like LaFeO_3 , LaMnO_3 has

nearly cubic lattice parameters, which make a structure solution and refinement very hard [37,34]. Elemans et. al. [38] were the first to report the $Pnma$ space group for pure LaMnO_3 . The oxygen stoichiometry of these AMnO_3 compounds is very sensitive to synthesis conditions. Stoichiometric LaMnO_3 is an antiferromagnetic insulator with a Neel temperature of 130K dominated by the strong Coulomb interactions between the electrons. The spins are ordered ferromagnetically in the ac plane with the spins parallel to a -axis [39]. There is an antiferromagnetic coupling between the layers, along the b -axis which is close to 180° [31].

2.4.2. Ionic view of electronic structure

Fig 2.2 shows the electronic configuration for the Mn^{3+} and Mn^{4+} ions in the compound AMnO_3 in a hybrid orbital structure. Mn ions have an incomplete d-shell (Mn: $[\text{Ar}] 3d^5 4s^2$). According to the Hund's rule, all the unpaired electrons in outer d-shell align their spins parallel to one another in order to minimize the energy. Thus only five d-levels corresponding to the majority spin are accessible.

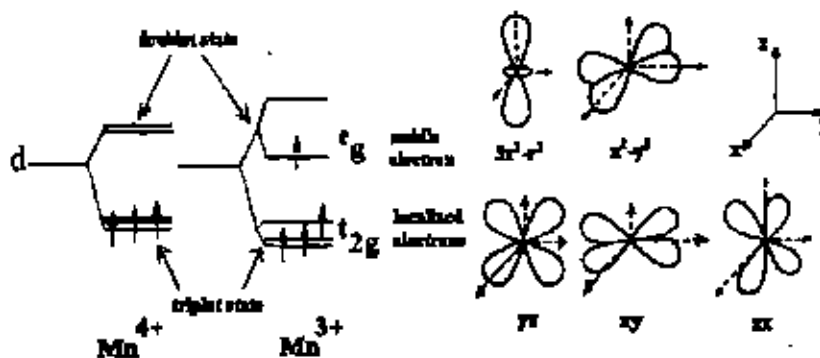


Figure 2.2: Electron states of the outermost $3d$ energy level of the Mn^{3+} and Mn^{4+} ions.

The five d levels are split in e_g (two degenerate levels , $d_{x^2-y^2}$ and $d_{3z^2-r^2}$) and t_{2g} (three degenerate levels , d_{xy} , d_{yz} and d_{zx}) due to the cubic crystal field . This splitting has been estimated to be around 1 eV [40]. John-Teller (JT) distortions act on Mn^{3+} leading to a further splitting. The two e_g levels are then separated in energy around 0.25 eV . The t_{2g} levels are also split due to JT distortions but this has not any relevance for the system as

the electrons living there are completely localized. Only the majority spins levels are shown. The minority spins levels are much higher in energy (due to Hund's coupling which can be several eV).

Hund's rule is implied by two interactions: coulomb repulsion makes electrons to be in a different d-orbital each; Hund's coupling obliges the electrons spins to be parallel. In isolated atoms, the five d-orbitals are degenerate but they split into three-fold degenerate (i.e. triplet state) t_{2g} (d_{xy} , d_{yz} and d_{zx}) and two-fold degenerate (i.e. doublet state) (for instance , $d_{x^2-y^2}$ and $d_{3z^2-r^2}$) orbitals as seen in Fig-2.2 , due to the cubic symmetry in which manganites crystallize [41] . The t_{2g} orbitals are lower in energy than the e_g orbitals because the later are aligned with the p-oxygen levels leading to a larger coulomb repulsion than in order directions. Mn^{4+} has three electrons in the outer d-shell that can be considered as localized in the three t_{2g} levels giving a total spin $S = 3/2$ (core spin). The two e_g levels remain empty. On the other hand, Mn^{3+} has an extra electrons that fills one of the e_g levels ($S = 2$). This single electron is unstable, however, and the system reduces its energy by splitting the doublet- state into two hyperfine energy levels. This well-known phenomenon, called the Jahn-Teller effect [42], is characteristic of Mn^{3+} ions and it has important consequences for the physical properties of manganites.

These e_g levels are the active ones for conductivity. These levels hybridize with oxygen p-levels [43] consisting the conduction band whose bandwidth depends on the overlapping of the e_g orbitals of the Mn and the p-levels of the oxygen. The minority (anti - parallel) spin levels are very high in energy . This implies that only majority spins can conduct. For this reason, manganites are called half- metals.

Fig-2.3 outlined the electronic hopping within narrow and fully spin-polarized bands are supported by a band structure calculation made for the end members of one dilution series, $LaMnO_3$ and $CaMnO_3$ [44]. For $LaMnO_3$ this calculation shows a typical separation between up and down polarized bands of about 1.5 eV and bandwidths of order 1-1.5 eV. Photoemission experiments on $La_{1-x}D_xMnO_3$ ($D= Ca, Pb$) confirm these basic features [45]. The density of states for such a system is shown schematically in the

figure. It has shown for comparison the density of states for Ni metal. Since the up and down spin bands are well separated, the magnetic polarization (saturation moment) is 100%, compared to 11% in Ni. This will lead to reversal of carrier spin direction across FM domains and large grain-boundary effects.

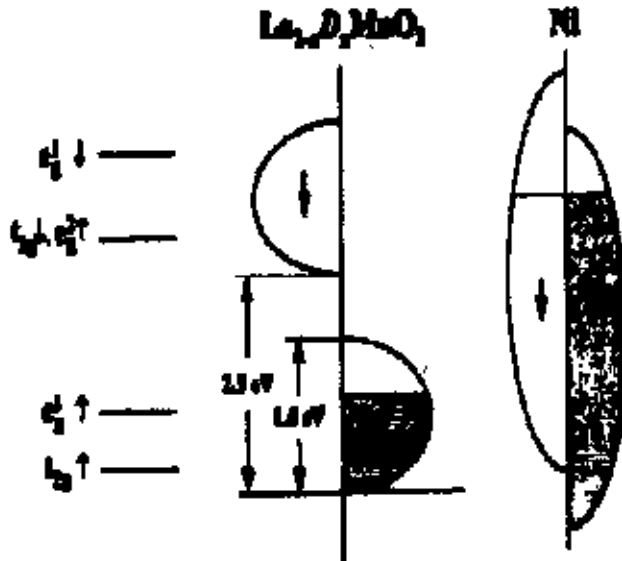


Figure 2.3: Schematic $T=0$ density of states for doped LaMnO_3 . The level diagram to the left shows the approximate positions of the 3d bands in undoped LaMnO_3 . The energy scale for $\text{La}_{2/3}\text{Sr}_{1/3}\text{MnO}_3$ is extracted from photoemission data. Comparison is made to Ni metal which possesses a much smaller degree of spin polarization.

2.4.3 Physical overview of doped manganites

The characteristic properties of doped perovskite manganites like the CMR effect and the strong correlation between the structure and electronic-magnetic phases can all be attributed to the ratio of the Mn^{3+} and Mn^{4+} ions. The parent compound crystallizes in AMnO_3 type perovskite structure having general formulas $\text{RE}_{1-x}\text{AE}_x\text{MnO}_3$, where RE stands for trivalent rare earth cation such as La, Pr, Nd, Sm, Eu, Gd, Tb, Y etc. and AE stands for divalent alkaline earth cation such as Ca, Sr, Ba etc. On this perovskite

like structure (RE, AE) occupies the vertices of the cubic unit cell, Mn occupies the body center and O occupies the six faces of the cube which forms MnO₆ octahedra.

The (RE,AE) site can in most cases form homogenous solid solution. Both the end members LaMnO₃ and CaMnO₃ are antiferromagnetic insulator having single valent Mn ions i.e. Mn³⁺ and Mn⁴⁺ respectively. On partial doping of the trivalent RE-ion by divalent alkaline earth cation AE, leads to the formation of a mixed valence state of the Mn i.e. Mn³⁺ and Mn⁴⁺ to maintain the charge neutrality of the system. The mixed valency of the Mn ions may also be controlled by varying the oxygen content. This doping with some divalent cation causes the structure to get distorted due to the differences in the size of the various atoms and leads to Jahn-Teller effect. Perovskite-based structures occasionally show lattice distortion as modifications from the cubic structure due to doping. One of the possible origin in the lattice distortion is the deformation of the MnO₆ octahedron arising from the Jahn-Teller effect that is inherent to high-spin (S=2) Mn³⁺ with double degeneracy of e_g orbital. Another lattice deformation comes from the connection pattern of the MnO₆ octahedra in the perovskite structure, forming rhombohedral or orthorhombic lattices. In these distorted perovskites, the MnO₆ octahedra show alternate buckling. Such a lattice distortion of the perovskite AMnO₃ (where A=RE_{1-x}AE_x) is governed by the Goldsmith tolerance factor 't' which measures the deviation from perfect cubic symmetry (t=1) and is defined as,

$$t = (r_D + r_O) / \sqrt{2}(r_T + r_O) = 1 \dots\dots\dots (2.2)$$

where r_D, r_T and r_O are the radii of the divalent, trivalent, and oxygen ions, respectively [46]. The tolerance factor measures the deviation from perfect cubic structure (t=1). By using mixtures of T= La, Pr, and Nd and D =Ca, Sr, Ba, and Pb, t can be varied, with the result that the perovskite structure is stable for 0.85 < t < 0.91. At finite doping, charge balance is maintained by a fraction, x, of Mn ions assuming a tetravalent, Mn⁴⁺ (d³), configuration in a random fashion throughout the crystal, with the remainder in the Mn³⁺ (d⁴) state presumably, D substitution is equivalent to hole doping, but thermo power and Hall effect disagree on the carrier sign in the paramagnetic state, suggesting that a simple band picture is not valid. Mixed valency can also be modified by varying

the oxygen content. For $x=0$ and 1, M ($T < 100\text{K}$) was found to be small, indicating an antiferromagnetic (AF) ground state.

At intermediate values of x , M rises and peaks with its Hund's-rule value at $x=0.3$. In subsequent work van Santen and Jonker showed that at temperatures above the ferromagnetic curie point, T_c , the resistivity behaves like a semiconductor, $d\rho/dT < 0$, but that below T_c , not only is there a sharp reduction in resistivity, but also a transition to metallic behaviour, $d\rho/dT > 0$ [20]. This behaviour is shown for $\text{La}_{1-x}\text{Sr}_x\text{MnO}_3$ and $\text{La}_{1-x}\text{Ca}_x\text{MnO}_3$ in figures 2.4 and 2.5.

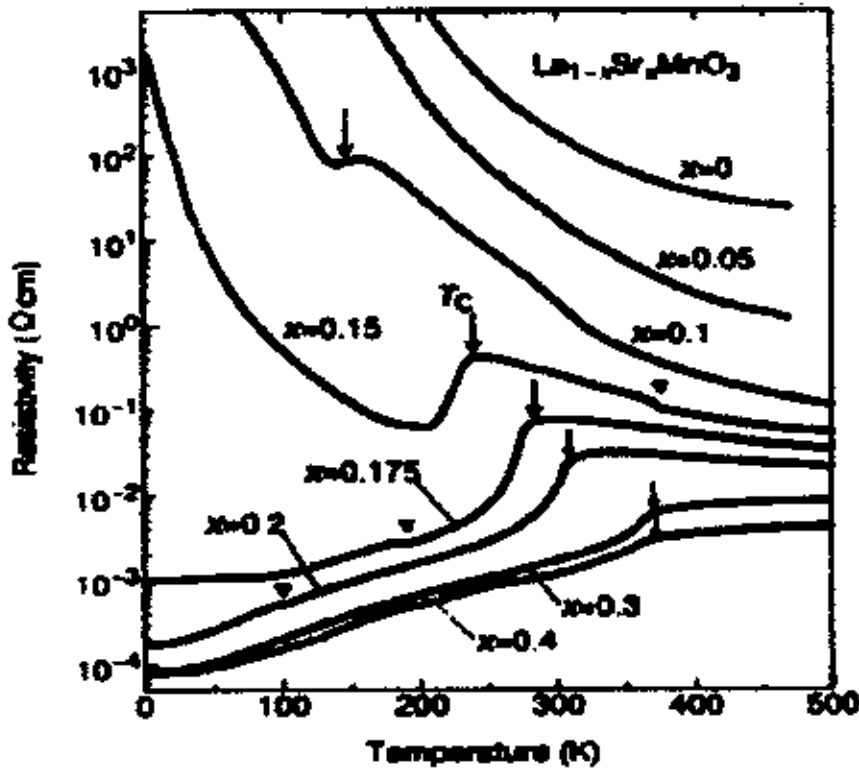


Figure 2.4: Resistivity against temperature for $\text{La}_{1-x}\text{Sr}_x\text{MnO}_3$ for various x values. The arrows denote the transition as determined by magnetization measurement.

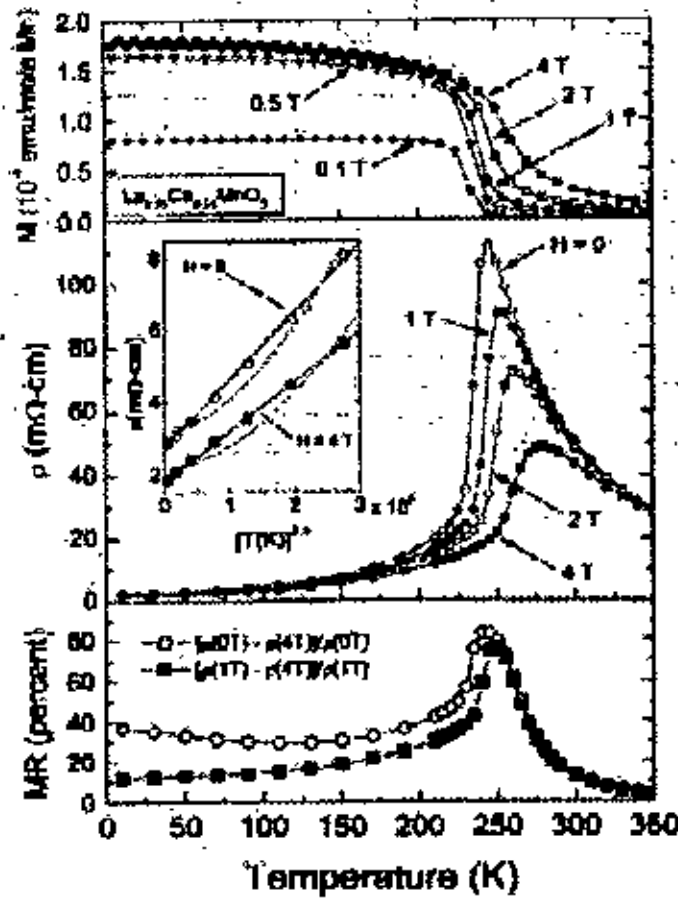


Figure 2.5: Top frame- magnetization against temperature for $\text{La}_{0.75}\text{Ca}_{0.25}\text{MnO}_3$ for varies field values. Middle frame resistivity against temperature. The inset shows the low temperature resistivity compared to $T^{2.5}$ (solid line) and $T^{4.5}$ (dashed line) behaviour. Bottom frame- magnetoresistance against temperature. Open symbols reflect low-field behaviour and solid symbols reflect the high field behaviour.

2.4.4. Layered manganese oxide perovskites

Three- dimensional perovskites manganese structure consists on a lattice of oxygen octahedral with a Mn ion in their center as seen in Fig.2.1(a), where the trivalent La^{3+} -site is substituted by divalent Sr^{2+} ion . Therefore, there is an oxygen ion between every two manganese as shown in the MnO_2 plane in Fig 2.1(b).The structure of these planes is completely analogous to the CuO_2 planes found in the cuprate high temperature

superconductors (HTSC's). The MnO_2 planes are then stacked in a variety of sequence with MnO_2 planes interleaved with (La, Sr)O planes in figure 2.6.

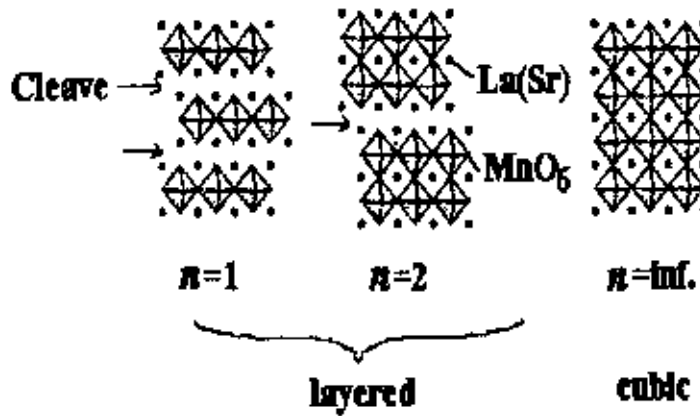


Figure 2.6: The crystal structure of the layered and cubic manganites.

The compounds are annotated depending upon how many MnO_2 planes are arranged between the bi-layer of (La, Sr)O planes. (La and Sr can be replaced by many other tri and divalent ions) This series is called the Ruddlesden-Popper (RP) series, and has the general formula $(\text{La,Sr})_{n+1}\text{Mn}_n\text{O}_{3n+1}$. The $n=1$ compounds have formula unit $(\text{La,Sr})_2\text{MnO}_4$ and are analogous to the HTSC compounds $(\text{La,Sr})_2\text{CuO}_4$. The $n=2$ compounds have the formula unit $(\text{La,Sr})_3\text{Mn}_2\text{O}_7$. The $n=\infty$ compounds have no (La,Sr)O bilayers, and have the formula unit $(\text{La,Sr})\text{MnO}_3$. They are cubic or distorted cubic compounds, and the most heavily studied of the manganites.

2.4.5. Transport properties of CMR materials

In magnetism, it is customary to distinguish an intrinsic property, which depends only on the bulk chemical composition and crystal structure, from extrinsic properties that are governed by the sample size and microstructure. For example, hysteresis is generally an extrinsic property, whereas on the other hand, spontaneous magnetization is an intrinsic property. Intrinsic properties are best measured on single crystal and epitaxial film. Magnetoresistance can be an intrinsic or an extrinsic property. Intrinsic magnetoresistance is maximum close to the ferro-paramagnetic transition and appears

due to the intrinsic interactions in the materials. The general form of the magnetization and the resistivity of CMR materials are shown in figure 2.7.

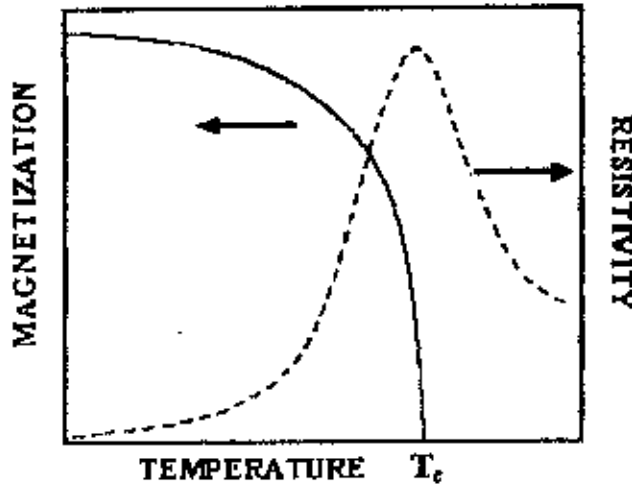


Figure 2.7: Resistivity and magnetization as a function of temperature.

When a magnetic field is applied, the peak on the resistivity moves toward higher temperature and dramatically decreases its height. As shown there the magnetic transition is accompanied by a change in the behaviour of the resistivity with temperature. The system is metallic below the magnetic critical temperature T_c ($dp/dr > 0$) and insulator in the paramagnetic region ($dp/dr < 0$). T_c ranges from the 15K for EuB_6 to more than 500 K for double perovskites. In particular, manganites cover a wide range of T_c (100–400K). Approaching T_c from below, the resistivity increases dramatically- sometimes by order of magnitude.

The polycrystalline samples show a completely different behaviour characterized by two features: a sharp increase of magnetoresistance at low field and at linear background at higher-fields. It has been suggested by Gupta et al [47], and Li et al.[48] that the low-field magnetoresistance, which is consistently observed in polycrystalline manganites, is due to spin-dependent scattering in grain boundaries. A low external field can readily rotate the grain magnetization into a parallel configuration and thereby cause a significant drop in resistivity and low-field magnetoresistance. The degree of spin polarization is

temperature dependent and increase with decreasing temperature [49]. Hwang et al.[50] suggested that the effect was due to spin-dependent tunneling between adjacent grains separated by an insulating grain boundary constituting a tunnel barrier for the spin-polarized conduction electrons. Also within this model the low-field magnetoresistance can be explained by the alignment of magnetizations of neighboring grains.

Spin-dependent scattering or spin-dependent tunneling can explain the low-field magnetoresistance but fail to explain the linear high-field magnetoresistance. Evetts *et al.* [51] suggested that the high-field magnetoresistance is associated with a magnetically mesoscopic disordered interface layer present in the vicinity of grain boundaries. The transport mechanism in the interface layer is the same as in the bulk parts of the grains, but the layer has depressed curie temperature and magnetization, which could be caused by strain, defects and weakened or absent bonds near the grain surface. The high-field MR could be related to alignment of spins in the disordered interface layer.

2.4.6 Comparison of magnetotransport of few other polycrystalline samples

Grain boundaries effects on the resistivity and magnetoresistance of polycrystalline manganites compounds were reported very early by Volger et al.[52]. The recent research was initiated by the work of Hwang *et al.*[50]and Gupta et al.[47]Hwang et al. elaborated the role of Grain boundary (GB's) in manganites by direct comparison of the MR and field-dependent magnetization at low temperature for single crystal and bulk polycrystalline samples of $\text{La}_{0.67}\text{Sr}_{0.33}\text{MnO}_3$.Mainly magnetization of $\text{La}_{0.67}\text{Sr}_{0.33}\text{MnO}_3$ single crystals and polycrystalline ceramics and $\text{La}_{0.67}\text{Ca}_{0.33}\text{MnO}_3$ and $\text{La}_{0.67}\text{Sr}_{0.33}\text{MnO}_3$ epitaxial and polycrystalline films respectively .Both investigation found that the resistivity and magnetoresistance depended sensitively on the microstructure, whereas magnetization was hardly affected it.

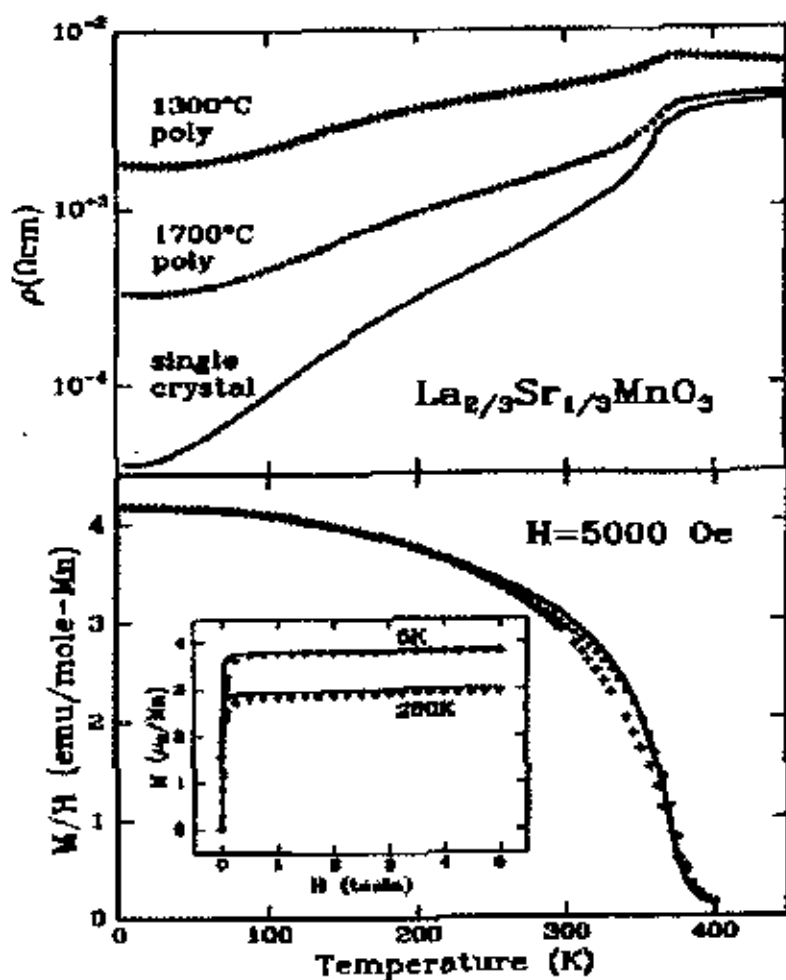


Figure 2.8: Top panel: zero-field resistivity of $\text{La}_{0.67}\text{Sr}_{0.33}\text{MnO}_3$ single crystal and polycrystals as a function of temperature. Bottom panel: magnetization of the samples as a function of temperature measured at $B=0.5 \text{ T}$. The inset shows the field-dependent magnetization at 5 and 280 K. (reproduced from Hwang et al. [50]).

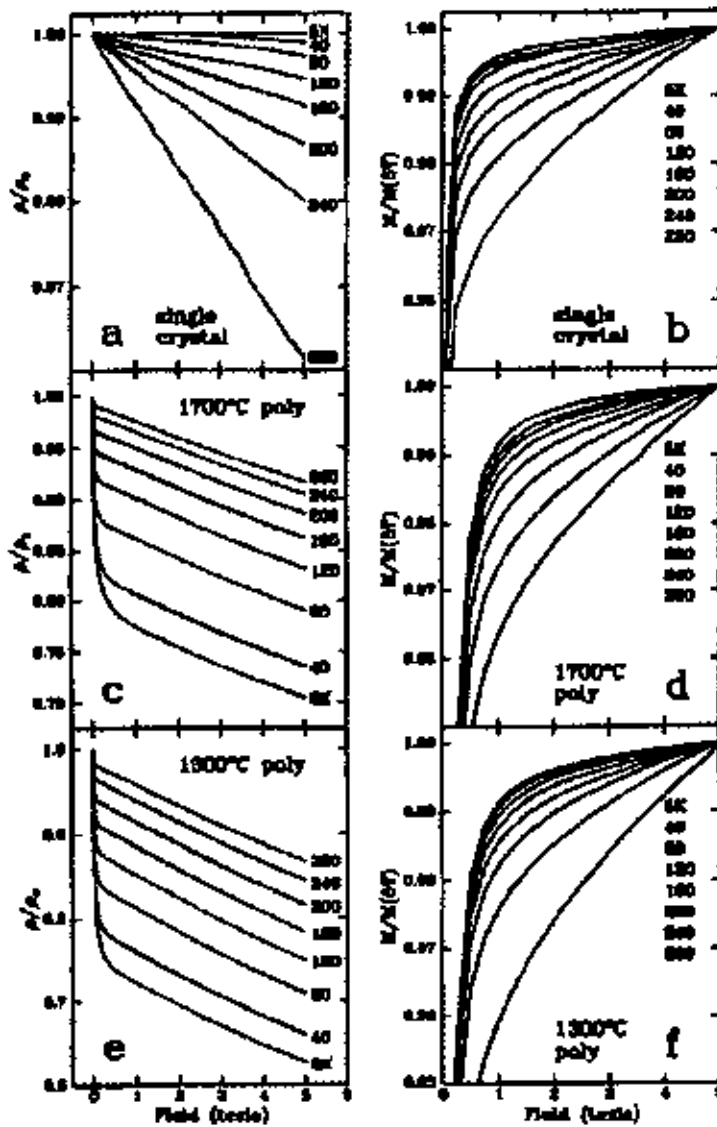


Figure 2.9: Magnetoresistance data of the samples of figure 13. Panels (a), (c) and (e): normalized resistivity ρ/ρ_0 as a function of magnetic field. ρ_0 denotes the zero-field resistivity. Panels (b), (d) and (f): magnetic field dependence of the normalized magnetization (reproduced from Hwang et al. [50]).

Hwang et al. [50] investigated an LSMO single crystal and two LSMO single crystal and two LSMO ceramic samples sintered at 1300 and 1700°C, respectively. The sample sintered at the higher temperature had the larger grain size. The data of Hwang et al. [50] are reported in figure 2.8 and 2.9.

Figure 2.8 shows the zero-field resistivity and the magnetization of the samples as a function of temperature. Whereas the low-temperature resistivity depends strongly on the microstructure, the magnetization of the three samples is virtually identical. The effect of the grain boundaries on the magnetoresistance is even more dramatic. Figure 2.9 shows the field dependent resistivity and magnetization of the samples investigated. Whereas the single crystal shows a magnetoresistance linear in magnetic field, the polycrystalline samples show a sharp drop at low magnetic fields followed by a linear dependence at higher fields. Again the field dependence of the magnetization is virtually identical for the three samples. The magnitude of the low-field magnetoresistance increases with decreasing temperature in contrast to the intrinsic magnetoresistance, that has a maximum near the curie temperature and decreases with decreasing temperature. These result cannot be explained by the intrinsic magnetoresistance alone, since the intrinsic magnetoresistance is only a function of the magnetization. Hwang et al.[50] suggested that the low-field magnetoresistance in polycrystalline samples is due to spin polarized tunneling between misaligned grains.

It was shown by Hwang et al [50] that, phenomenologically one has to distinguish weak and strong links between the grains. Only weak links give rise to a considerable low-field magnetoresistance. Whereas the micro structural characteristics of the two types of links are not clear, the formation of weak or strong links can be controlled by the fabrication conditions.

2.4.7: Intrinsic and extrinsic magnetoresistance

In this section the intrinsic and extrinsic magnetoresistance is discussed and also illustrate how they can be distinguished from experiment. Some results from the literature are used for exemplification.

Intrinsic magnetoresistance

Intrinsic magnetoresistance is maximum close to the ferromagnetic-paramagnetic transition and appears due to the intrinsic interactions in the materials.

Figure 2.10 shows the temperature dependence of the zero field and an applied field of 5T resistivities of a single-crystalline thin film $\text{La}_{0.7}\text{Ca}_{0.3}\text{MnO}_3$ sample (data obtained from Hundley et al.[53]).The corresponding magnetoresistance, $\text{MR}=\rho_{H}/\rho_{0-1}$, is shown in the same graph. This sample has no internal grain boundaries so the magnetoresistive response is therefore entirely intrinsic.

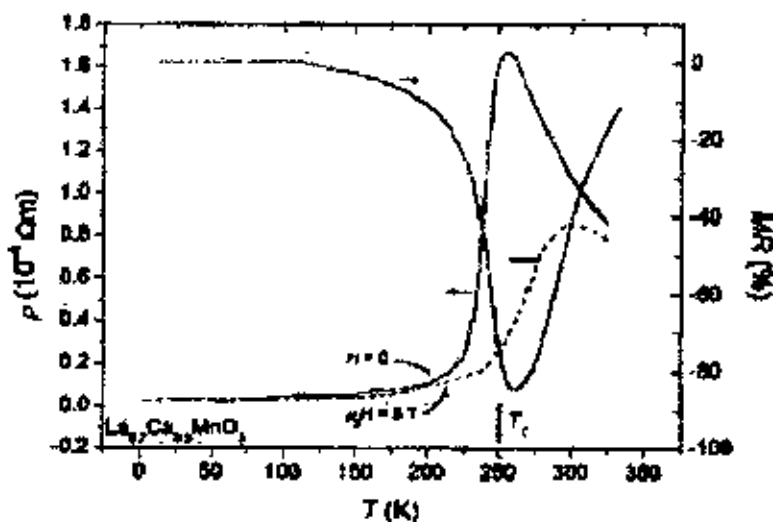


Figure 2.10: Resistivity of single-crystalline thin-film $\text{La}_{0.7}\text{Ca}_{0.3}\text{MnO}_3$ in zero magnetic field and in an applied field of 5T. The graph shows also the corresponding magnetoresistance. Adopted from Hundly et al. [53].

The thin-film substance shows a metal-to-insulator transition coinciding with the ferromagnetic-to-paramagnetic transition at the temperature (250K).Qualitatively, the temperature dependence of the magnetoresistance can be explained in terms of Zener's double-exchange mechanism. The simplest expression for conductivity is $\sigma = ne\mu$, where n is the number of carries, e is their charge, and μ their mobility. The metal-to-insulator transition could thus originate from either a change of the number of carriers or a change the mobility of the carriers. In the double-exchange theory the change of hopping mobility is the dominant effect on the conductivity .The transfer integral for electron transport between adjacent Mn sites is $t=t_0\cos(\theta/2)$ where θ is the angle between the spin directions of the two Mn cores spins. Below the ferromagnetic transition temperature the spin system is ferromagnetically ordered and the probability for electron transfer (and

thereby the mobility) is high. The zero-field resistivity shows metallic-like temperature dependence with a positive slope. Around the Curie temperature the spin system becomes disordered because the thermal energy exceeds the ferromagnetic exchange energy. The hopping amplitude decreases and a drastic increase of the zero-field resistivity is observed. Above T_c the resistivity decreases with temperature as expected for an insulator, where transport is thermally activated. The sample exhibits a large negative magnetoresistance peaking just above the Curie temperature. Below T_c the spins align spontaneously and the external field has little influence on θ . The magnetoresistance gradually vanishes when the magnetic moment approaches its saturation value. Near T_c , however, the spin system is highly susceptible to the external field, which causes a substantial change of the local spin disorder and thereby of the carrier mobility. Thus, the field drives the material more metallic. Far above the Curie point the external field can no longer compete with the thermally induced random spin fluctuations and the magnetoresistive response decreases with temperature.

Many research groups have suggested that double exchange alone is not sufficient in order to explain the CMR. The models proposed evoke a competition between double exchange and another mechanism—such as polaron formation due to the strong electron-phonon coupling or localization by spin fluctuations; this competition is supposed to drive the metal-insulator transition. The balance between the two competing mechanisms is very sensitive to an applied magnetic field that suppresses spin fluctuations and enhances the ferromagnetic order. The debate on the essential transport mechanism in the manganites has not yet been decided.

It has been also suggested by Coey et al.[54] or Von Helmlolt et. al.[55] that the very large change in resistivity observed for manganites is due to magnetic polaron formation in the paramagnetic regime. The e_g electrons may induce a local polarization of its neighboring spins forming a small ferromagnetic entity called a magnetic polaron. According to their suggestion a magnetic polaron can be considered a quasi-particle and it can jump from lattice site to lattice site carrying along its spin polarization. This hopping takes place via thermal activation. Below the Curie temperature (or when a magnetic field is applied) the magnetic polarons are destroyed. This could contribute to the abrupt change of resistivity

near T_c . Another kind of polarons, which could be present in manganites, are dielectric polarons formed due to the coulomb interaction between the electron and its surrounding ionic charges. The concept of polaron transport in mixed-valence manganites is not yet fully understood.

In theoretical results by Millis et al. [56] the resistivity was obtained from a dynamical mean-field calculation including double exchange and a coupling of carriers to phonons. The calculations show that the resistivity above T_c can be tuned from semiconducting to metallic on decrease of the electron-phonon-coupling strength.

Extrinsic magnetoresistance

Figure 2.11(a) compares the temperature dependence of magnetoresistance of a single-crystalline manganite (an epitaxial thin film) with that of a polycrystalline thin film having the same composition ($\text{La}_{0.67}\text{Ca}_{0.33}\text{MnO}_3$). Data was obtained from (Gupta et al. [47])

Both samples show a magnetoresistance maximum near the curie temperature, which can be ascribed to intrinsic magnetotransport (the CMR effect). For the epitaxial film the magnetoresistance vanishes at low temperatures, as expected for a single-crystalline material. However, the polycrystalline film shows an increasing magnetoresistance with decreasing temperature.

Figure 2.11(b) shows the field dependence of magnetoresistance at two different temperatures below the ferromagnetic transition temperature. The epitaxial sample shows a linear variation of the magnetoresistance with the applied field. This indicates that the Bloch wall motion and rotation in single-crystalline manganites do not dominate transport. The magnetoresistance varies smoothly through the region of domain rotation, which takes place in low fields, so the increasing magnetoresistance is mainly due to enhanced magnetic order. The magnetoresistance effect is small and decreases with decreasing temperature. The polycrystalline sample exhibits a completely different behavior characterized by two features: 1) a sharp increase of magnetoresistance at low fields followed by 2) a linear background at higher fields. The slope of the high-field

contribution is broadly temperature independent. The low-field magnetoresistance, which is often termed LFMR, increases with decreasing temperature.

It has been suggested by Gupta et al.,[47] and Li et al.[48] that the low-field magnetoresistance, which is consistently observed in polycrystalline manganites, is due to spin-dependent scattering in grain boundaries. In ferromagnetic metals the exchange energy splits the conduction band into majority and minority carrier bands resulting in a spin imbalance at the Fermi level. In mixed-valance manganites the majority and the minority bands are separated by an energy gap arising from the strong intra-atomic coupling between the 3d e_g conduction electrons and the 3d t_{2g} core spins[57]. The spin polarization may therefore approach 100% at low temperatures (thus, manganites may be characterized as half-metals). In the ferromagnetic state each grain in a polycrystalline manganite may constitute a single magnetic domain.

In the virgin state, where no field is applied, the grains have their magnetic moments randomly oriented. The polarized conduction electrons are easily transferred between Mn sites within a magnetic domain. However, an electron traveling across a grain boundary to an adjacent grain (or domain) may become subject to a strong spin dependent scattering leading to a high zero-field resistivity. A low external field can readily rotate the grain magnetization into a parallel configuration and thereby cause a significant drop in resistivity and low-field magnetoresistance. The degree of spin polarization is temperature dependent and increases with decreasing temperature [49].

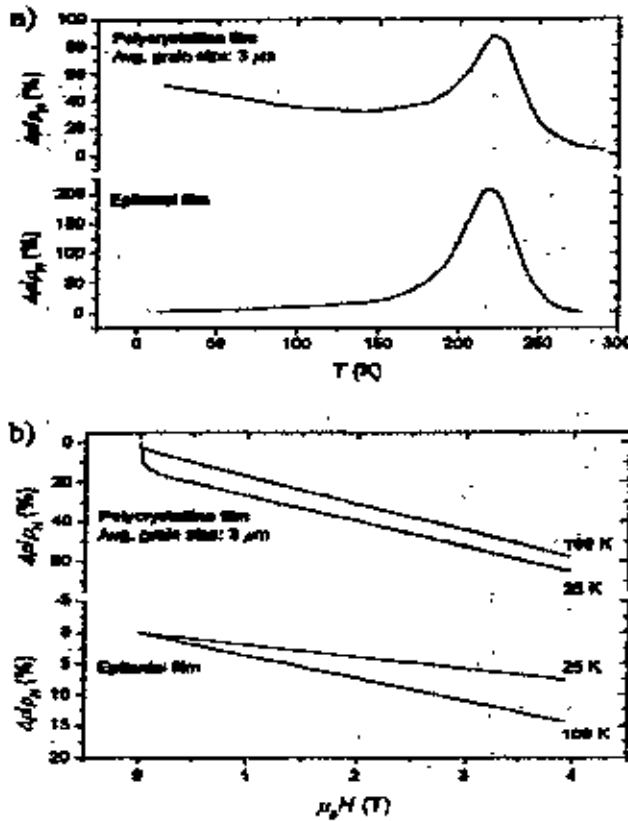


Fig 2.11: Magnetoresistance for a field change of 0 to 2T versus temperature of poly-crystalline (top panel) and epitaxial (bottom panel) thin film $\text{La}_{0.67}\text{Ca}_{0.33}\text{MnO}_3$. b) magnetoresistance as a function of applied field taken at 25 and 100K.

This could explain why the low-field magnetoresistance becomes more and more dominant as the temperature is decreased. Spin-dependent scattering of polarized conduction carriers is the dominant mechanism describing spin-valve effects in metallic GMR multilayers [58].

Hwang et al. [50] offered a different explanation to the low-field magnetoresistance effect observed below the Curie temperature. They compared the magnetoresistive properties of single-crystalline and polycrystalline $\text{La}_{0.67}\text{Sr}_{0.33}\text{MnO}_3$ and also observed LFMR (low field magnetoresistance) in the polycrystalline samples, which was absent in the single crystal. They suggested that the effect was due to spin-dependent tunneling between adjacent grains separated by an insulating grain boundary constituting a tunnel

barrier for the spin-polarized conduction electrons. Also within this model the low-field magnetoresistance can be explained by the alignment of magnetizations of neighboring grains.

Spin-dependent scattering or spin-dependent tunneling can explain the low-field magnetoresistance but fail to explain the linear high-field magnetoresistance. Evetts et. al. [51] suggested that the high-field magnetoresistance is associated with a magnetically mesoscopic disordered interface layer present in the vicinity of grain boundaries (fig 2.12). The transport mechanism in the interface layer is the same as in the bulk parts of the grains, but the layer has depressed curie temperature and magnetization, which could be caused by strain, defects and weakened or absent bonds near the grain surface. The high-field MR could be related to alignment of spins in the disordered inter-face layer.

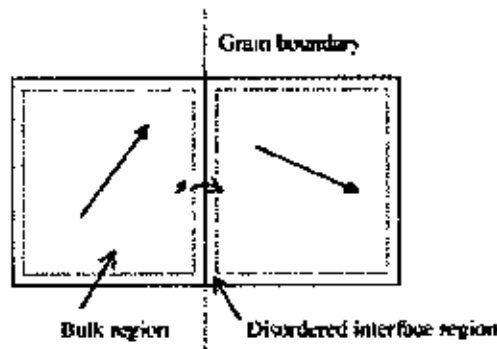


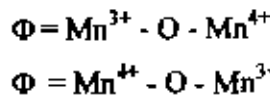
Figure 2.12: Schematic illustration of grain-boundary transport in a polycrystalline mixed-valence manganite.

Figure 2.12: Schematic illustration of grain-boundary transport in a polycrystalline mixed-valence manganite. Each grain constitutes a single magnetic domain. The conduction electrons show a high degree of spin polarization inside the grains. When traveling across the grain boundary conduction electrons may be subject to a strong spin-dependent scattering, which can be reduced if a low external magnetic field aligns the magnetizations of the two grains. Spin alignment in the disordered surface layers gives rise to high-field magnetoresistance.

2.5 Classical double exchange model

Jonker and Santen discovered the strong correlation between ferromagnetism and metallic conductivity in doped manganites. That ferromagnetism is arising from an indirect coupling between the manganese ions (Mn^{3+} , Mn^{4+}) via the cations.

In the parent compound $LaMnO_3$, the manganese (Mn) ion is a trivalent oxidation (Mn^{3+}) state having electronic configuration $3d^4$ with three electrons occupy the t_{2g} levels and are coupled to a core spin $S = 3/2$ by the strong intraatomic Hund's coupling and the fourth electron (itinerant) occupies one of the energetically degenerate e_g orbitals. The basic idea of double exchange is that the configurations,



are degenerate leading to a delocalization of the hole on the Mn^{4+} site or electron on the Mn^{3+} site.

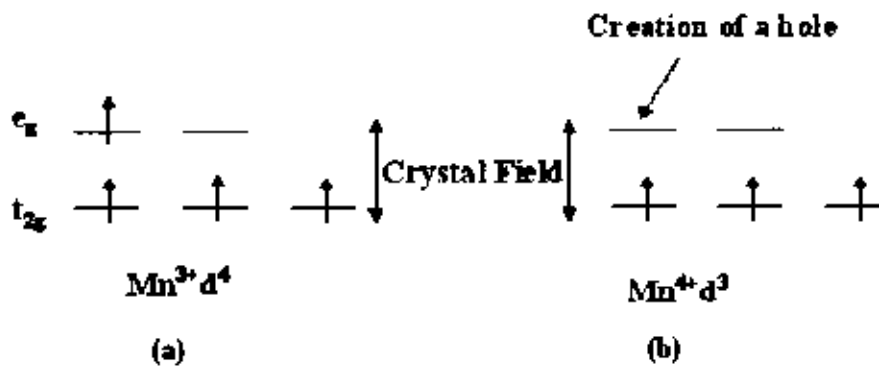


Figure 2.13. The splitting of the t_{2g} and e_g band in $La_{1-x}A_xMnO_3$

The transfer of an electron simultaneously from Mn^{3+} to O^{2-} and from O^{2-} to Mn^{4+} , this process is a real charge transfer process and involves overlap integral between Mn and O orbitals. Because of strong Hund's coupling JH , the transfer matrix element has finite value only when the core spins of the Mn ions aligned ferromagnetically. The Hund's coupling

of degenerate state lifts the degeneracy and the system resonates between Φ_1 and Φ_2 if the core spins are parallel, leading to simultaneous occurrence of metallic conductivity and ferromagnetism.

2.5.1 Importance of classical double exchange model

The double exchange (DE) model can explain the transport properties of manganites qualitatively. This mechanism is very important for understanding the complex behaviour of manganites. This classical model has been deeply studied and in certain regimes, qualitative agreement with experiments has been found. In particular, magnetic properties are better described than electric properties (there is not a metal – insulator transition for DE). But some manganites, as hole doped $\text{La}_{1-x}\text{Sr}_x\text{MnO}_3$, are metallic for the whole range of temperatures Fig 2.14. The fact is that lattice distortions compete with the bandwidth (as is the case of $\text{La}_{1-x}\text{Sr}_x\text{MnO}_3$) implies a more efficient double-exchange interaction. In fact, Varma [59] and, more recently, Lyanda-Geller *et al.* [60] have pointed out that Jahn-ellor phonons are not necessary to get the metal insulator transition and double-exchange plus disorder, which leads to localization as proposed. Moreover double-exchange has shown a much richer phenomenology than expected in the beginning.

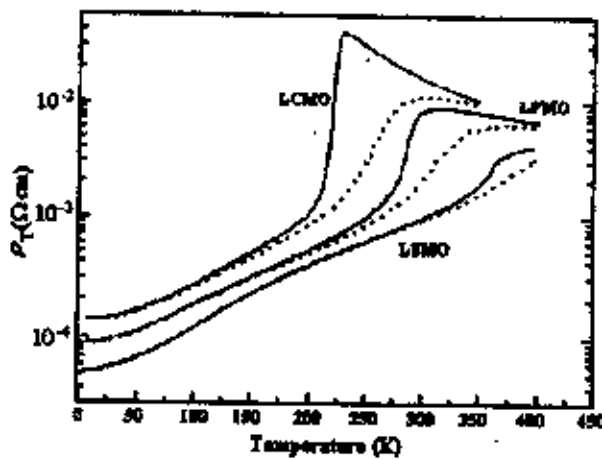


Figure 2.14: Temperature dependences of resistivity under zero magnetic field (solid lines and under 7T dotted lines for $\text{La}_{0.7}\text{Ca}_{0.3}\text{MnO}_3$, $\text{La}_{0.67}(\text{Ca,Pb})_{0.33}\text{MnO}_3$ and $\text{La}_{0.7}\text{Sr}_{0.3}\text{MnO}_3$ [59].

2.5.2 Drawbacks of double exchange models and subsequent theories

Although double exchange mechanism is clearly important for understanding the behaviour of manganites perovskite, it is not enough [61,62,63]. This model alone would not be able to explain the experimental facts. It can not explain its high resistivity fast doping dependency, and incorrect behaviour in resistivity for $T < T_c$. DE can not describe the huge magnitude of the CMR effect, underestimates the resistivity values in the paramagnetic phase by several orders and can not account for the existence of various antiferromagnetic phases, charge / orbital ordering, phase separation scenario and strong lattice effects/anomalies seen experimentally due to its inherent limitation for several manganites. Millis et al. [63] incorporated the idea that double exchange alone does not explain the resistivity of $\text{La}_{1-x}\text{Sr}_x\text{MnO}_3$. They calculated the resistivity within the double-exchange model including spin fluctuations and found that resistivity decreases below T_c and a positive magnetoresistance above T_c , both features in contradiction to the experimental results. They also argued that the electron-phonon coupling due to the dynamic Jahn-Teller distortion plays an important role, and that a strong interplay between electron-phonon coupling, including charge localization, and Hund's coupling, generating a FM metallic phase, is responsible for the observed properties of manganites.

2.5.3 Jahn - Teller distortion

The double exchange (DE) is the basic mechanism underlying the transport properties of the manganites. This exchange is not sufficient to explain the experimental results. The strong electron-phonon coupling in manganites is mainly caused by the Jahn-Teller (JT) effect of Mn^{3+} . The JT effect causes local distortion of the crystal structure in which some of the MnO bonds become shorter and other longer. This breaks the local cubic symmetry and splits the degeneracy of the e_g levels on that site. By occupying the orbital with the lowest energy, the e_g electron can become effectively self-trapped to form together with the surrounding deformed lattice and a quasi-particle called lattice polaron or Jahn-Teller polaron. This transport of lattice and spin distortions is also called as magnetic - polaron. Calculation by Millis et al. [64] predict the localization of charge carriers by temporal and spatial JT distortions around and above T_c . This would lead to

the observed activated resistivity behaviour in the paramagnetic phase below T_c , the self-trapping of carriers ends leading to a relaxation of the lattice and an enhancement of the conductivity. In this theory JT coupling and DE are needed to explain the properties in the various magnetic phases. This leads to the prediction of lower more correct T_c values, and can explain the high resistivity and large CMR effect in manganites. Simply lattice distortion occurs due to their different atomic sizes, crystal structure and different magnetic moments.

Distorted perovskite cubic structure showed in fig 2.1. A simple inspection is enough to discover sources for distortion. Cations A and B can have very different sizes, producing tilting and twisting of the oxygen octahedral [67-69]. This distortion can be estimated by the so called Goldschmidt tolerance factor:

$$\Gamma = \frac{r_{MN} + r_O}{\sqrt{2}(r_{A/B} + r_O)} \dots\dots\dots(2.3)$$

where r is the sizes of the different ions in the system. $\Gamma = 1$ for a cubic lattice and decrease as the difference in size between A and B increases. It has been found that for oxides and fluorides the perovskite structure types are stable in the below range

$$1.0 \geq \Gamma \geq 0.77$$

Tilting of the octahedral can be measured with the distortion of the Mn-O-Mn bond angle θ and $\theta = 180^\circ$ for cubic symmetry. For particular compositions, θ can range 150° to 180° . Orbital overlapping decreases with the distortion and the relation between the W and θ has been estimated as $W \propto \cos^2 \theta$ [70]. Bandwidth is closely related to the magnitude of the critical temperature T_c which could be increased by chemical pressure, namely, by choosing the right cations A and B (or, equivalently, by the application of external pressure). Two parameters are important here, the mean value of the cation sizes $\langle r_{A/B} \rangle$ and its variance $\sigma^2 = \langle r_{A/B}^2 \rangle - \langle r_{A/B} \rangle^2$ [68]. In the ideal case $\sigma^2 = 0$, a T_c as large as 520K could be achieved. Another source of distortion to be taken into account is the

larger size of Mn^{3+} (~ 0.72) respect to Mn^{4+} (~ 0.5). This leads to a breathing distortion mode as shown in Fig -2.15.

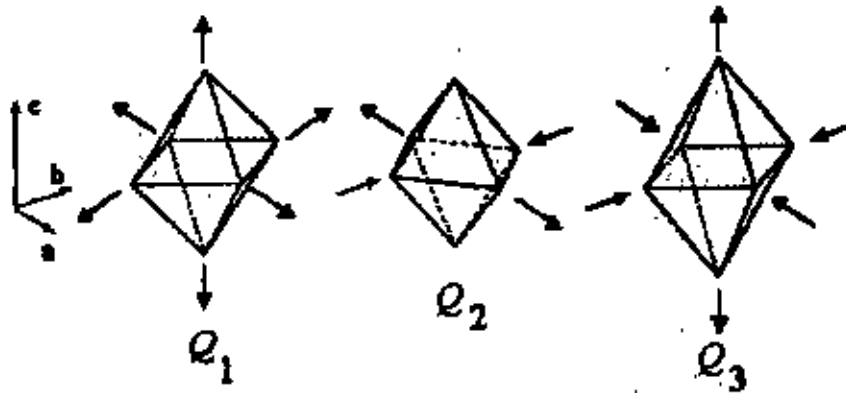


Figure 2.15: Q_2 and Q_3 are the two Jahn – Teller modes of distortion of the oxygen octahedral associated to the splitting of the e_g levels of Mn^{3+} [71]. These particular cases correspond to $Q_2 > 0$ and $Q_3 > 0$ is the breathing distortion that occurs due to the different sizes of Mn^{4+} and Mn^{3+} .

Only two type of distortion (modes of vibrations) are relevant for the splitting of e_g doublet i.e. JT distortion: Q_2 and Q_3 which are shown in Fig 2.15. The Q_3 is a tetragonal distortion which results in elongation or contraction of MnO_6 octahedra. However in case of manganites the effective distortion is the basal plane distortion (called as Q_2 mode) in which one diagonally opposite O pair is displaced outwards and the other pair displaced inward. As Mn^{4+} does not have an electron in the e_g states, it will not act as JT ion .Lattice distortion of the octahedral can be static or dynamic. When the carriers have certain mobility, the distortion of Mn^{3+} and Mn^{4+} ions is random and changes with time. Therefore, electron – phonon coupling arises and, in fact, Millis et al.[64].and Roder et al.[72] have claimed that it is necessary to take account if the lattice vibration to explain the change in curvature of the resistivity close to T_c .Moreover , due to large Hunds coupling , magnetic polarons can be formed [64] . The localization of the carrier in lattice and/or magnetic polarons can explain the activated behaviour of the resistivity for $T > T_c$.When the bandwidth is narrow; the localization induced by lattice deformations is much relevant and leads to charge/orbital ordering and stripe formation [73,74].

2.5.4 Phase diagram and resistivity

Phase diagram of doped perovskite manganites are exceptionally rich with different magnetic as well as structural phases. The phase diagrams that have been established so far for different compounds e.g. $\text{La}_{1-x}\text{Ca}_x\text{MnO}_3$, $\text{La}_{1-x}\text{Ba}_x\text{MnO}_3$, $\text{La}_{1-x}\text{Sr}_x\text{MnO}_3$ etc. are constructed from detailed measurements of macroscopic physical quantities such as resistivity, susceptibility and magnetization on single crystal and bulk ceramic samples [75]. Even though the phase diagram of each composition is different due to the variation in sizes of different atoms involved but they have some common features. $\text{La}_{1-x}\text{Ca}_x\text{MnO}_3$ is a good candidate material for basic understanding and hence its phase diagram has been described in detail. CMR manganites are oxides of the type $\text{R}_{1-x}\text{A}_x\text{MnO}_3$, where R denotes a rare earth and A is a divalent, often alkaline earth element. Much interest has been devoted to the CMR manganites, since these displays a diversified phase diagram.

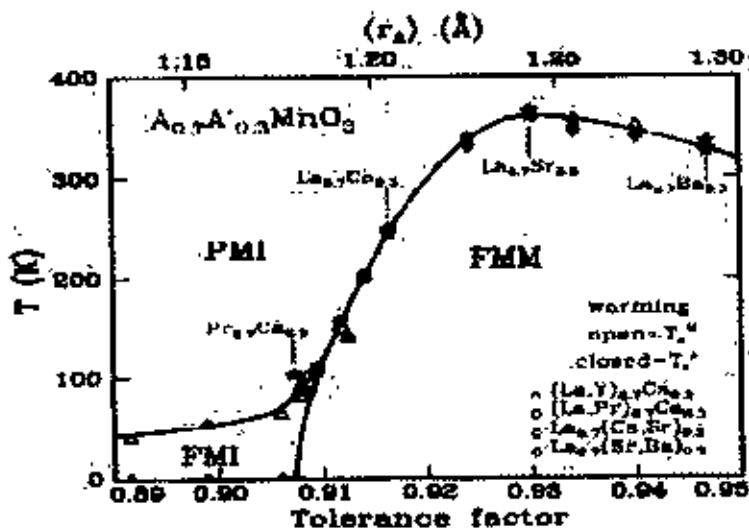


Figure 2.16 Phase diagram of temperature versus tolerance factor for $\text{A}_{0.7}\text{A}'_{0.3}\text{MnO}_3$, where A is a trivalent ion and A' a divalent ion. Open symbols denote T_C determined by magnetization measurements and closed symbols denote T_C determined by resistivity measurements. All data were taken while warming.

In figure 2.16 at low temperature the resistivity is metallic, rising sharply while going through the ferromagnetic transition and showing semiconducting behavior in the paramagnetic phase in the case of Ca doping, whereas the resistivity in the case of Sr

doping remains metallic above the curie temperature .accordingly , the ferromagnetic transition in this case compound is accompanied by a metal- insulator transition as evidence by the resistivity rise and the negative temperature coefficient of the resistivity in most compounds above T_c .

2.6 Models of manganites

Perovskite manganites have a large potential for applications based on their various physical and chemical properties [76,77]. The magnetic field sensitivity of the transport properties, the strong metal insulator transition at the curie temperature, the electric field polarizability of the material and its subsequent effect on the transport properties, the half metallicity of the electronic bands, etc. are properties of the rare earth manganites that could be exploited in a variety of devices. Based on the properties, a number of device approaches are being explored and few of them are described below.

(1) The magnetoresistance of manganites might be used in magnetic sensors, magnetoresistive read head, and magnetoresistive random access memory. Magnetic sensors can be made from either thin films or single crystals and can be used to sense the magnitude of a magnetic field in one or several directions by choosing the right crystal form and de- magnetizing factor. A good low field magnetoresistive response however, can be obtained in manganite samples with a high density of grain boundaries and in tunnel spin valve structures. One of the first working devices of this kind was constructed by Sun et al.[78].

(2) The electric field effect has also been observed in manganites. Here the top layer can be paramagnetic, such as $SrTiO_3$ [79], or a ferroelectric layer, such as $PbZr_{0.2}Ti_{0.8}O_3$ and the bottom layer is a CMR material, but the changes are more profound is the case of $PbZr_{0.2}Ti_{0.8}O_3$ where only 3% change in the channel resistance is measured over a period of 45 min at room temperature which makes this material attractive for nonvolatile field – effect device application [80,81].

(3) The large temperature coefficient of resistance (TCR) calculated as $(1/R)(dR/dT)$ just below the resistivity peak makes these CMR materials interesting for use in bolometric detectors [82-84]. Bolometer is an instrument for detecting and measuring radiation

(4) Since the properties of the CMR materials are quite spectacular at reduced temperatures, i.e. below 100 K, so at these low temperatures, the combination of high- T_c superconducting cuprates thin films and CMR manganites could lead to Hybrid HTSC-CMR structures [85,86].

(5) Chemical applications include catalysis such as catalysis for automobile exhausts, oxygen sensors and solid electrolytes in fuel cells. The catalytic activity is associated with the $Mn^{3+} - Mn^{4+}$ mixed valence and the possibility of forming oxygen vacancies in the solid [87,88].

2.7 Magnetic-based device

Recent progress in oxide perovskites thin film technology has led to the discovery of a large negative magnetoresistance at room temperature which open up new avenues for applications in diverse area of technology such as magnetic random access memories and reads heads for hard disc drives. Based on the properties of manganites, a number of device approaches are being explored, some of which are discussed here briefly.

- (i) Magnetic field sensors (a) using the CMR effect in a film, (b) using a spin valve structure and (c) as a microwave CMR sensors. The industrial requirements for a magnetic sensor are operation at room temperature and up to 400 K, at least a 20% MR at a field ~ 10 mT applied field, temperature dependent CMR values over 350 ± 50 K and acceptable noise values. The current thinking is that oxide-based CMR sensors will have maximum impact only on memory systems approaching densities of 100 GB cm^{-2} .

- (ii) Electric field effect devices (a) using a SrTiO_3 gate and (b) using a ferroelectric gate. Field effect transistors (FET) based on CMR channels show some interesting characteristics depending on the dielectric layer on top as to whether it is a paraelectric layer such as STO, or a ferroelectric layer such as PZT. The advantage of these devices unlike conventional NVRAM would be that the reading of the state of the memory would be direct since the resistance is considerably different.

- (iii) Low temperature hybrid *HTS-CMR* devices: As the properties of *CMR* materials are quite spectacular at reduced temperatures, i.e., below 100K, there may some advantages to integrating them with *HTS* devices.

- (iv) Room Temperature Bolometric Infrared (*IR*) Sensors: Due to the advance in thermoelectric cooling, materials with high thermal nonlinearities in the temperature range of 250 to 300 K are potential candidates for bolometric sensors.

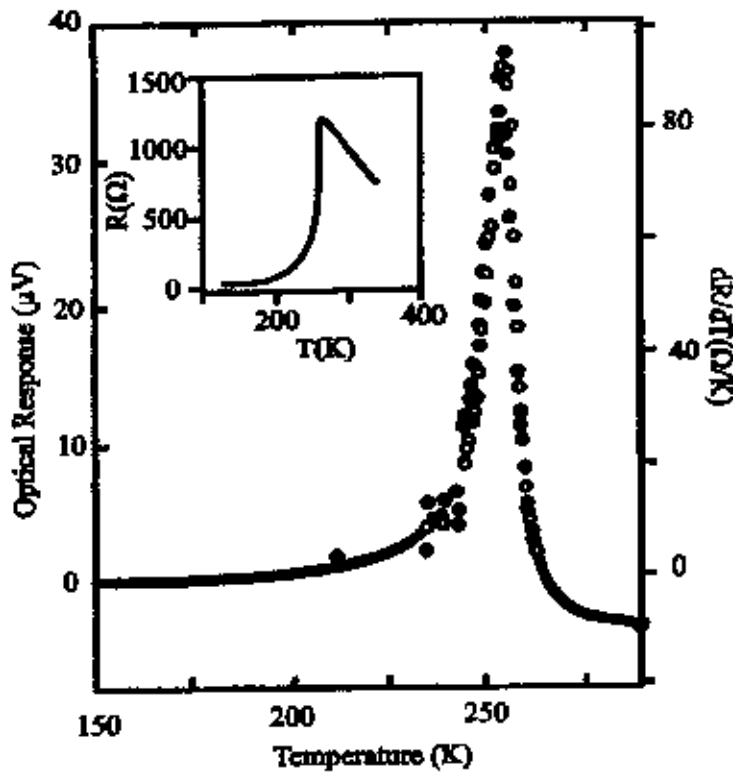


Figure 2.17: Optical response of a film of LCMO (closed circles) in comparison with the TCR (open circles). The curve is shown in the inset.

The commercial bolometers based on VO_x used now a days use temperature coefficient of resistance (TCR) values around 2.5% to 4%. In comparison TCR values ranging from 8% to 18% are possible in the LCMO manganites over the same temperature range (figure, 2.17).

Reference

- [1] Chahara K, Ohno T, Kasai M, and Kozono Y, "Magnetoresistance in magnetic manganese oxide with intrinsic antiferromagnetic spin structure", *Appl. Phys. Lett.* **63**, (1993).
- [2] von Helmholtz R, Wocker J, Holzappel B, Schultz M, and Samwer K, "Giant negative magnetoresistance in perovskite like $\text{La}_{2/3}\text{Ba}_{1/3}\text{MnO}_3$ ferromagnetic films", *Phys Rev Lett* **71**, 2331(1993).
- [3] Jin S, Tiefel T H, McCormack M, Fastnacht R A, Ramesh R, and Chen J H, "Thousand-fold change in resistivity in magnetoresistive La-Ca-Mn-O films", *Science* **264**, 413 (1994).
- [4] Baibich M N, Broto J M, Fert A, Nguyen Van Dau F, Petroff F, Etienne P, Creuzet G, Friederich A, and Chazeles J, "Giant magnetoresistance of (001) Fe/(001) Cr magnetic superlattices," *Phys. Rev. Lett.* **61**, 2472 (1988).
- [5] Binasch G, Grunberg P, Saurenbach F, and Zinn W, "Enhanced magnetoresistance in layered magnetic structures with antiferromagnetic interlayer exchange". *Phys Rev B* **39**, 4828(1989).
- [6] Parkin S S P, Li Z G, and Smith D J, "Giant magnetoresistance in antiferromagnetic Co/Cu multilayers," *Appl. Phys. Lett.* **58**, 2710 (1991).
- [7] Parkin S S P, More N, and Roche K P, "Oscillations in exchange coupling and magnetoresistance in metallic superlattice structures: Co/Ru, Co/Cr, and Fe/Cr" *Phys Rev Lett* **64**, 2304 (1990).
- [8] Parkin S S P, Bhadra R, and Roche K P, "Oscillatory magnetic exchange coupling through thin copper layers", *Phys Rev Lett* **66**, 2152(1991).
- [9] Berkowitz A E, Mitchell J R, Carey M J, Young A P, Zhang S, Spada F E, Parker F T, Hutten A, and Thomas G , *Phys Rev Lett* **68** 3745(1992).
- [10] Xiao J Q, Jiang J S, and Chien CL, "Giant magnetoresistance in nonmultilayer magnetic systems", *Phys Rev Lett* **68**, 3749 (1992).
- [11] Hylton T L, Coffey K R, Parker M A, and Howard J K, *Science* **261**, 1021 (1993).

- [12] Girtlemaun J I, Goldstein Y, and Bozowski S, "Magnetic Properties of Granular Nickel Films", *Phys Rev B* **5**, 3609 (1972).
- [13] Helman J S, and Abeles B, *Phys Rev Lett* **37**, (21) 1429 (1976).
- [14] Parkin S S P, and York B R, "Technical Article - Spin-Polarized Current in Spin Valves and Magnetic Tunnel Junctions", *Appl Phys Lett* **62**, 1842 (1993).
- [15] Grunberg P, Schreiber P, Pang Y, Brodsky M B, and Sower H, "Layered Magnetic Structures: Evidence for Antiferromagnetic Coupling of Fe Layers across Cr Interlayers", *Phys Rev Lett* **57**, 2442(1986).
- [16] Parkin S S P, *Annu Rev Mater Sci* **25**, 357(1995).
- [17] Pippard A B, "Magnetoresistance", Cambridge University Press Cambridge UK (1984).
- [18] Watts S M, Wirth S, von Molnar S, Barry F, and Coey J M D, "Evidence for two-band magnetotransport in half-metallic chromium oxide", *Phys Rev B* **61**, 149621 (2000).
- [19] Ashcroft N, and Mermin B, "Solid State Physics" Holt Rinehart and Winston New York (1976).
- [20] Jonker G H, and van Santeen J H, "Ferromagnetic compounds of manganese with perovskite structure", *Physica* **16**, 337 (1950).
- [21] van Santeen J H, and Jonker G H, "Electrical conductivity of ferromagnetic compounds of manganese with perovskite structure", *Physica* **16**, 599 (1950).
- [22] Jonker G H, and van Santeen J H, "Magnetic compounds with perovskite structure iii. Ferromagnetic compounds of cobalt ", *Physica* **19**, 120 (1953).
- [23] Voĭgar J, "Further experimental investigations on some ferromagnetic oxidic compounds of manganese with perovskite structure", *Physica* **20**, 49 (1950).
- [24] Jonker G H, "Semiconducting properties of mixed crystals with perovskite structure", *Physica* **20**, 1118 (1954).
- [25] Wollan E O, and Koehler W C, " Neutron diffraction study of the magnetic properties of the series of perovskite-type compounds [(1-x) La, x Ca] MnO₃", *Phys. Rev.* **100**, 545 (1955).
- [26] Vratistva S, and Zajicek J, *Phys Stat Sol (a)* **52** K 39 (1979).
- [27] Pollert E, Krupicka S, and Kuzmicova E, "Structural study of Pr_{1-x}Ca_xMnO₃ and Y_{1-x}Ca_xMnO₃ perovskites", *J Phys Chem Solids* **43**, 1137 (1982).

- [28] Kusters R M, Singleton J, Keen D A, McGreevy R, and Hayes W, "Magnetoresistance measurements of the magnetic semiconductor $\text{Nd}_{0.5}\text{Pb}_{0.5}\text{MnO}_3$," *Physica B* **155**, 362 (1989).
- [29] Ju S, Sun H, and Li Z "Study of magnetotransport in polycrystalline perovskite manganites", *Journal of Physics Condensed Matter*, **14**, L631 (2002).
- [30] Prinz G.A., "Magnetoelectronics," *Science* **282**, 1660 (1998).
- [31] Goodenough J B, "Magnetism and the Chemical bond", (Huntington: Krieger) (1970).
- [32] Zener C, "Interaction between d shells in the transition metals", *Phys. Rev.* **81**, 440 (1951).
- [33] Zener C, "Interaction between d shells in the transition metals. ii. Ferromagnetic compounds of manganese with perovskite structure", *Phys. Rev.* **82**, 403 (1951).
- [34] van Aken B B, "Structural response to electronic transitions in hexagonal and ortho-manganites", Ph D Thesis, Dutch foundation for Fundamental Research on Matter (MOF), University of Groningen, Netherlands, (2001).
- [35] Naray-Szabó S V, *Naturwissenschaften* **31**, 466 (1943)
- [36] Yakel H L, *Acta Crystallogr.* **8**, 394 (1955)
- [37] Rodríguez-Martínez L M, and Attfield J P, "Disorder-induced orbital ordering in $\text{La}_{0.7}\text{MnO}_3$ ", *Phys. Rev. B* **63**, 024424 (2001).
- [38] Elemans JBAA, van Laar B, van der Veen K R, and Loopstra B O, "The crystallographic and magnetic structure of $\text{La}_{1-x}\text{Ba}_x\text{Mn}_{1-x}\text{Mg}_x\text{O}_3$ ", *J. Solid State Chem.* **238** (1971).
- [39] Huang Q, Santoro A, Lynn J W, Rrwin R W, Borchers J A, Peng J L, and Greene R L, "Structure and magnetic order in undoped lanthanum manganite", *Phys. Rev. B* **55**, 14987 (1997).
- [40] Tokura Y., "Colossal magnetoresistance oxides,"(Gordon & Breach Monographs in Condensed Matter Science, London, 1999).
- [41] Pickett W E, and Singh D J, "Electronic structure and half-metallic transport in the $\text{La}_{1-x}\text{Ca}_x\text{MnO}_3$ system", *Phys. Rev. B* **53**, 1146 (1996).

- [42] Alvysdas Lisauskas, "Low frequency noise in thin film colossal magnetoresistance", Ph D Thesis, Department of Condensed Matter Physics at the Royal Institute of Technology, Sweden. (2000).
- [43] Pickett W E and Singh D J, "Electronic structure and half-metallic transport in the $\text{La}_{1-x}\text{Ca}_x\text{MnO}_3$ system", *Phys. Rev. B* **53**, 1146 (1996).
- [44] Satpathy S, Popovic Z S, and Vukajlovic F R, "Origin of charge orbital order in the half-doped manganites", *Phys. Rev. Lett.* **76**, 960 (1996).
- [45] Park J H, Chen C T, Cheong S W, Bao W, Meigs G, Chakarian V, and Idzerda Y U, "Electronic aspects of the ferromagnetic transition in manganese perovskites", *Phys. Rev. Lett.* **76**, 4215 (1996).
- [46] Ziese M and Thornton M J, "Spin Electronics", Springer Heidelberg (2001).
- [47] Gupta A, Gong G Q, Xiao G, Duncombe P R, Lecoœur P, Trouilloud P, Wang Y Y, Dravid V P, and Sun JZ, "Grain boundary effects on the magnetoresistance properties of perovskite manganite films", *Phys. rev. B*, **54** (22), R15629 (1996).
- [48] Li X W, Gupta A, Xiao G, and Gong G Q, "Low-field magnetoresistive properties of polycrystalline and epitaxial perovskite manganite films", *Appl. Phys. Lett.*, **71** (8), 1124 (1997).
- [49] Ju S, Sun H, and Li Z, "Study of magnetotransport in polycrystalline perovskite manganites", *Journal of Physics Condensed Matter*, **14**, L631 (2002).
- [50] Hwang H Y, Cheong S W, Ong N P, and Batlogg B, "Spin-Polarized Intergain Tunneling in $\text{La}_{2/3}\text{Sr}_{1/3}\text{MnO}_3$ ", *Phys. Rev. Lett.* **77**, 2041 (1996).
- [51] Evetts J E, Blamire M G, Mathur N D, Isaac S P, Teo B, Cohen L F, and Macmanus-Driscoll J L, "Defect-induced spin disorder and magnetoresistance in single-crystal and polycrystal rare-earth manganite thin film", *Philosophical Transactions of the Royal Society, London A*, **356**, 1593 (1998).
- [52] Volgar J, "Further experimental investigations on some ferromagnetic oxidic compounds of manganese with perovskite structure", *Physica* **20**, 49 (1950).
- [53] Hundley M F, Hawley M, Heffner R H, Jia Q X, Neumeier J J, and Teamer J, "Transport-magnetism correlations in the ferromagnetic oxide $\text{La}_{0.7}\text{Ca}_{0.3}\text{MnO}_3$ " *Appl. Phys. Lett.* **67** (6), 860 (1995).

- [54] Coey J M D, Viret M, and Von Molnar S, "Mixed-valence manganites", *Advances in physics*, 48(2) 167,(1999).
- [55] Von Helmlolt R, Wecker J, Haupt L, and Barner K, "Intrinsic giant magnetoresistance of mixed valence La-A-Mn oxide (A=Ca,Sr,Ba)", *J. Appl. Phys.* 76 (10) 6925 (1994).
- [56] Millis A J, Mueller R, and Shraiman B I, "Fermi-liquid to polaron crossover: Double exchange and the physics of colossal magnetoresistance", *Phys. Rev. B* 54 5405 (1996).
- [57] Okimoto Y, Ishikawa T, Katsufuji T, Urashibara A, Arima T, and Tokura Y, "Anomalous variation of optical spectra with spin polarization in double-exchange ferromagnet: $\text{La}_{1-x}\text{Sr}_x\text{MnO}_3$ ", *Phys. Rev. Lett.* 75(1), 109,(1995).
- [58] Tumanski S, "Thin film magnetoresistive sensors" Bristol: Institute of Physics Publishing (2001).
- [59] Layanda-Geller Y., Chun S.H., Salamon M.B., Goldbart P.M., Han P.D., omioka Y.T, Asamitsu A., and Tokura Y., "Charge transport in manganites : hopping conduction, the anomalous hall effect and the universal scaling," cond-mat/0012462(2000)
- [60] Ananth Hegde and Ashwini Dwarkanath, "Emerging memory technology" CSE597E,www.cse.psu.edu.tyts.
- [61] Millis A.J., Littlewood P.B.,and Shraiman B.I., "Double exchange alone does not explain the resistivity of $\text{La}_{1-x}\text{Sr}_x\text{MnO}_3$," *Phys.Rev.Lett.* 74,5144(1995).
- [62] Roder H., Zang J., and Bishop A.R., "Lattice effects in the colossal magnetoresistance manganites," *Phys.Rev.Lett* 76, 1356(1996).
- [63] Zang J., R.Bishop A., and Roder H., "Double degeneracy and Jahn-Teller effects in colossal- magnetoresistance perovskites," *Phys Rev B* 53,R8840(1998).
- [64] Millis A J *Nature* 392 147. (1998)
- [65] Millis A J Shruiman B I and Mueller R *Phys Rev Lett* 77 175. (1996)

- [66] Millis A J, Mueller R and Shraiman B.I., “ Fermi – Liquid to polaron crossover double exchange and the physics of the colossal magnetoresistance”. *Phys Rev B* **54**, 5405.(1996)
- [67] Fontcuberta KJ., Martinez B., Seffar, A. Pinol S., Garcia-Munoz J.L., and Obradors X., “Colossal magnetoresistance of ferromagnetic manganites: structural tuning and mechanisms,” *Phys Rev Lett.* **76**,1122(1996).
- [68] Roderiguez-Martinez L.M., and Atfield, J.P. “Disorder-induced orbital ordering in $\text{La}_{0.7}\text{MnO}_3$,” *Phys Rev B* **63**, 024424 (2001).
- [69] Radaelli P.G., Iannone G., Marezio M., Hwang H.Y., Cheong S.-W., Jorgensen J.D., and Argyriou D.N., “Structural effects on the magnetic and transport properties of perovskite $\text{A}_{1-x}\text{A}_x\text{MnO}_3$ ($x=0.25,0.30$),”*Phys Rev B* **56**,8265(1997).
- [70] Garcia-Munoz J.L., Fontcuberta J., Suaaidi M., and Obradors X, “Band-width narrowing in bulk $\text{La}_{2/3}\text{A}_{1/3}\text{MnO}_3$ magnetoresistive oxides,” *J.Phys. :Condens.Matt.* **8**,L787(1996).
- [71] Kanamori J., “Crystal distortion in magnetic compounds,” *J Appl.Phys.* **31**,148(1996)
- [72] Roder H,Zang J and Bishop A.R. “Lattice effect in the colossal magnetoresistance”. *Phys Rev Lett* **74** 1356(1996).
- [73] van den Brink J, Khaliullin G and Khomskii D I cond-matt/0206053 “Colossal Magnetoresistance” T Chatterji (ed) Kulwer Academic Publishers Dordrecht Netherlands (2004).
- [74] Rao CNR, Arulraj A, Cheetham AK and Raveau B *J Phys: Condens Matter* **12** R83. (2000)
- [75]Chcong SW and Hwang HY Ferromagnetism vs Charge/Ordering in Mixed-Valent Manganites, in “Colossal Magnetoresistance Oxides” Y Tokura (ed.) Godon and Breach London. (2000)
- [76] Haghiri-Gosnet AM and Renard JP. *J Phys D:Encyclopedia of Nanoscience and Nanotechnology* vol X HS Nalwa (ed) pp 1-18 (and reference therein). (2003)

- [77] Venkatesan T, Rajeswari M, Dong ZW, Ogale SB and Ramesh R *Philos Trans Roy Soc A* 356 1661. (1999)
- [78] Sun JZ, Gallagher WJ, Duncombe PR, Krusin-Elsbaum L, Altoman RA, Gupta A, Lu Y, Gong GQ and Xiao G *Appl Phys Lett* 69 3266. (1996)
- [79] Ogale S B, Talyansky V, Chen C, Ramesh R, Greene R L and Venkatesan T *Phys Rav Lett* 77 1159. (1996)
- [80] Mathews S, Ramesh R, Venkatesan T and Benedetto J *Science* 276 238. (1997)
- [81] Es-Souni M, Girdauskaite E, Iakovlev S, Solterbeck CH and Zaporozhchenko V J *Appl Phys* 96 5691. (2004)
- [82] Choudhary R J, Ogale S A, Shinde S R, Hullavarad S Ogale S B, Bathe R N, Patil Sland Kumar R *Appl Phys Lett* 84 3846. (2004)
- [83] Rajeswari M, Chen C, Goyal A, Kwon C, Robson M C, Ramesh R Venkatesan T and Lakeou S. *Appl Phys Lett* 68 3555. (1996)
- [84] Lisauskas A, Khartsec S I and Grishin A. *Appl. Phys Lett* 77 756. (2000)
- [85] Goyal A, Rajeswari M, Shreekala R, Lofland S E, Bhagat S M, Boettcher T, Kwon C, Ramesh R and Venkatesan T. *Appl Phys Lett* 71 2535. (1997)
- [86] Chen ZY, Biswas A, Zutic I, Wu T, Ogale S B, Green R L and Venkatesan t *Phys Rev B* 63 212508. (2001)
- [87] Mcevoy S J *J Mater Sci* 36 1087. (2001)
- [88] Mori M, Sammes N M, Suda E and Takeda Y. *Solid State Ionics* 164 1. (2003)
- [89] Ramirez A.P., "Collossal Magnetoresistance," *J. phys., Condens. Matter* 9 8171 (1997)
- [90] Nagaev, E.L., "Physics of magnetic semiconductors." *Phys. Uspekhi* 39,781 (1996).

Chapter-3

Sample preparation and characterization

Experimental methods of sample preparation and characterization technique employed in synthesis of manganese oxide materials are described briefly in this chapter. The apparatus that we used in the measurements also described here.

3.1 Preparation of the samples

Samples can be prepared mainly using any of the following method:

1. Solid state reaction method.
2. Solution method.
3. Melt- quenched or glass ceramic method.
4. Thin film method.

3.1.1 Solid state reaction method

In solid state reaction method appropriate amounts of two or more chemicals are carefully grind together and mixed thoroughly in a mortar and pestle or ball mills. Grinded powders are then calcined in air or oxygen at a temperature above 750°C for several hours. This process is continued for several times until the mixture is converted into the correct crystalline phase. This calcined material are then grinded to fine powders and pelletized in a hydraulic press followed by sintering at different temperature below the melting point of the materials in air or any controlled atmosphere.

3.1.2. Solution method

In this method appropriate amount of solid chemicals are at first dissolved in nitric acid. This solution is then dried and then followed by calcination and sintering treatments. Some times water soluble materials such as nitrates are used for synthesizing superconducting ceramic materials. The nitrates are dissolved in water and then dried and calcined in a way similar to the solid state reaction method.

3.1.3 Melt-quenched or glass ceramic method

In this method appropriate amounts of mixed powder are taken in oxide or carbonate crucible and calcined for one to two hours below the melting point of the material. After calcinations the powders are melted at few hundred-degree celsius above the melting temperature and held there for a couple of hours. The melts are then poured into a cold iron or brass plate and pressed quickly by another plate to 1 to 2 mm thick sheets. The glasses thus obtained are then annealed at suitable temperature for different periods of time in air or in any controlled atmosphere.

3.1.4 Thin film method

Thin films of superconducting materials have been very successfully fabricated using the procedure like, evaporation, sputtering, ion beam sputtering, laser evaporation etc. Evaporation is conceptually the simplest of all the deposition techniques. In practice, however, some of the most sophisticated apparatus are used to evaporate epitaxial films of materials under very controlled conditions and these systems are more accurately called molecular electron beam epitaxy system (MBE/EBE). The technique involved utilizes a vacuum system to remove most of the contaminating gases from the deposition chamber. Typical pressures that are obtained in simple evaporations are in the 10^{-7} torr range until the MBE/EBE system requires pressures of less than 10^{-10} torr. The elements or compounds to be evaporated are heated in crucibles by either resistive heating elements or by electron beam heating. Typical evaporations have more than one evaporation source, and it is possible to obtain systems with as many as six independent sources. The high temperature produced in these sources cause the vapor pressure of the evaporation rise to a level at which a significant amount of these materials can be collected on a substrate that is located on a direct optical path from the evaporate. The substrate can typically be at a variety of temperatures, ranging from 77K to approximately 1300K depending on the required microstructure of the final film. The substrate materials are sapphires Al_2O_3 , MgO, silicon etc.

3.2.1. Material synthesis and sample preparation

In the present investigation samples were prepared using conventional solid state reaction method. Appropriate amounts of two or more chemical compounds are carefully mixed and grinding in a mortar or pestle or by ball milling with acetone for homogenization. Ground powders are then calcined in air or in oxygen at a temperature above 1373 K (1100⁰C) for several hours to remove the unwanted oxides present in the chemicals. Then these are reground and reheated. This process is continued until the mixture is converted into the correct crystalline phase. This calcined material are then ground to fine powders and palletized in a hydraulic press afterwards sintering at different temperatures except below the melting point of the materials in air or any controlled atmosphere.

Solution method, glass ceramic method, thin film method etc. are some of the common methods which used for the preparation of the sample.

3.2.2. Physicals properties

To study the samples physical properties they need to be characterized in different ways. In the present investigation, powder X-ray diffraction is employed to characterize homogeneity of the crystalline power. It would be provide the necessary feedback to improve the preparations method of the grown materials.

3.2.3. Preparation of the present samples

Polycrystalline samples were prepared using the conventional Solid –State reaction technique. Stoichiometric amounts of raw materials La₂O₃ (99.99%) , Dy₂O₃ (99.99%) , SrCO₃ (99.99%) , MnCO₃ (99.99%) , Fe₂O₃ (99.99%) , NiO (99.99%) were well mixed then calcined at 1100⁰C in air for 24 hours . The resulting powder samples were then reground and sintered at 1100⁰C for 48-50 hours in air with one intermediate grinding. Before the final sintering step at 1100⁰C for 24 hours, the samples were pressed into pellets. The pallets was placed in an alumina boat and inserted into the furnace for sintering and oxidation. All the pallets were sintered at 1100⁰C in the furnace in air atmosphere. The resulting pellets were subjected to electric and magnetic investigation. The specimen's crystallinity and structure were checked by X-ray diffractometry.

3.2.4. Methodology

The DC electrical resistivity for various polycrystalline samples was measured from room temperature down to liquid nitrogen temperature using standard four-probe method. The temperature dependence of normalized resistivity, ρ/ρ_0 at zero applied magnetic field for various polycrystalline samples and the corresponding behavior in presence of 0.7T applied magnetic field have been investigated. Magnetoresistance measurements were carried out in a magnetic field of around 0.7T in the temperature range 78 K to 300 K.

3.3. Lattice planes and Bragg's law

X-rays interact with electrons in atoms. When x-ray photons collide with electrons, some photons from the incident beam will be deflected away from the direction where they originally travel, much like billiard balls bouncing off one another. The scattered x-rays carry information about the electron distribution in materials. And the inelastic scattering process (Compton Scattering), x-rays transfer some of their energy to the electrons and the scattered x-rays will have different wavelength than the incident x-rays.

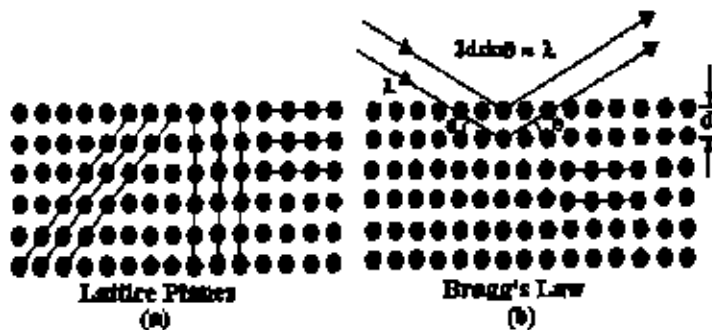


Figure 3.1: Bragg's law of diffraction. (a) Different forms of lattice planes, (b) Different forms atoms.

The peaks in an X-ray diffraction pattern are directly related to the atomic distance. Let us consider an incident X-ray beam interacting with the atoms arranged in a periodic

manner as shown in figure 3.1. The atoms, represented as black spheres in the graph, can be viewed as forming different sets of planes in the crystal (lines in graph on (a)).

For a given set of lattice plane with an inter – planner distance of d , the condition for a diffraction to occur can be simply written as lattice

$$2d_{hkl}\sin\theta=n\lambda$$

This is known as Bragg's law. Where, λ is the wavelength of the X-ray, θ is the scattering angle and n is an integer representing the order of the diffraction peak.

3.4. The van der Pauw method

The van der Pauw technique [1,2] is based on four point measurements, provided that certain condition are fulfilled:

- The contacts should be on the circumference of the samples (or very close to the boundary as possible)
- The contacts should be sufficiently small (or as close as possible)
- The sample is to be homogeneous and thin relative to the other dimensions
- The surface of the sample is to be singly connected, i.e. the sample should not have isolated holes.

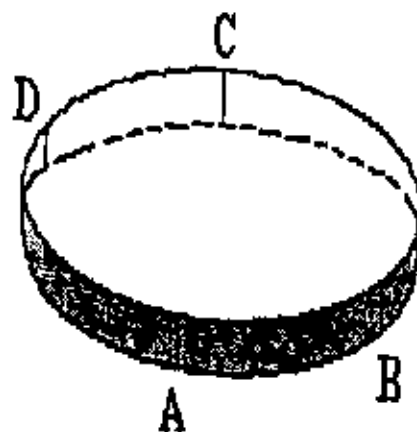


Figure 3.2: The four electrical contacts on the circumference of the discs shaped samples

Figure 3.2 shows the four contacts on the circumference of the disc shaped (irregular shaped) sample.

For a fixed temperature, we define resistance $R_{AB,CD}$ as the potential difference is $V_D - V_C$ between the contacts D and C per unit current I_{AB} through the contacts A and B. The current enters the sample through the contact A and leaves it through the contact B.

$$R_{AB,CD} = V_D - V_C / I_{AB} \dots \dots \dots (3.1)$$

$$R_{BC,DA} = V_A - V_D / I_{BC} \dots \dots \dots (3.2)$$

Van der Pauw technique is based on the theorem that between $R_{AB,CD}$ and $R_{BC,DA}$ there exists the simple relation:

$$\exp\left(-\frac{\pi d}{\rho} R_{AB,CD}\right) + \exp\left(-\frac{\pi d}{\rho} R_{BC,DA}\right) = 1 \dots \dots \dots (3.3)$$

Where d is the thickness of the uniform dice shaped sample and ρ is the resistivity of the material. If d and the $R_{AB,CD}$ and $R_{BC,DA}$ are known, then in Eq 3.3, ρ is the only unknown quantity .

In the general case, it is not possible to express ρ explicitly in known functions. The solutions can, however, be written in the form

$$\rho(T) = - \frac{\pi d}{\ln 2} \left(\frac{R_{AB,CD} + R_{BC,DA}}{2} \right) f \left(\frac{R_{AB,CD}}{R_{BC,DA}} \right) \dots \dots \dots (3.4)$$

Where f is a factor which is a function only of the ratio $R_{AB,CD}/R_{BC,DA}$ and satisfies the relation

$$\cosh \left\{ \frac{\left(\frac{R_{AB,CD}}{R_{BC,DA}} \right) - 1}{\left(\frac{R_{AB,CD}}{R_{BC,DA}} \right) + 1} \right\} = \frac{1}{2} \exp \frac{\ln 2}{f} \dots \dots \dots (3.5)$$

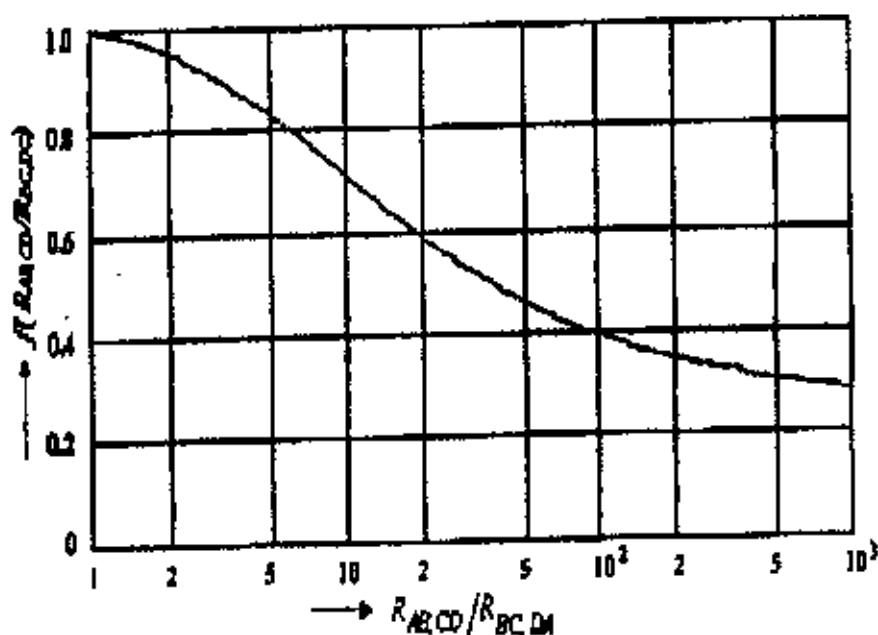


Figure 3.3: The function $f(Q)$ for determining the resistivity of the sample.

If we assume $R_{ABCD}/R_{BCDA}=Q$, then eq. 3.5 becomes

$$\frac{Q-1}{Q+1} = \frac{f}{\ln 2} \arccos h \left\{ \frac{\exp(\ln 2 / f)}{2} \right\} \dots \dots \dots (3.6)$$

A plot of the function is shown in figure 3.3.

3.5: Apparatus used for the present investigation

3.5.1 Description of liquid nitrogen cryostat

A liquid nitrogen cryostat is designed for the purpose of low temperature magneto-transport measurements. It is made up of nonmagnetic concentric stainless steel tubes. It consists of two parts (upper part and lower part) and each part consists of three concentric tubes of three different dimensions. The outer diameter of the upper part of the cryostat is 7.6 cm and inner diameter is 3.2 cm. The outer diameter for lower part is 3.8 cm and inner diameter is 3.2 cm. It has three chambers as shown in Figure 3.1. Outer chamber is called vacuum chamber the middle one is cryogen (liquid nitrogen) chamber and the

innermost chamber is sample space. Thickness of the wall of each chamber is about 0.2 cm. In the top of the second chamber there are two small pipes connected over the stainless steel plate of upper part of the cryostat, one for inlet of liquid nitrogen and the other for outlet of nitrogen gas. The lower part (20 cm long and 3.8 cm diameter) of the cryostat is shorter and narrower compared to the upper part (85 cm long and 7.6 cm diameter). It is made in such a way that the lower part of the cryostat can easily move between the pole pieces of the home made electromagnet. A stainless steel plate connects the lower part and upper part. The top of the upper part is sealed by another stainless steel plate. In the innermost chamber (sample space) there is a sample rod which is made up of stainless steel tube and a flat copper bar. The diameter of the sample rod is chosen in such a manner that it can easily move through the sample space. The top of the sample rod and innermost tubes are air tight connected with a union socket. A thermocouple is used for the measurement of temperature of the sample. It was observed that if the cryostat is filled with liquid nitrogen than it takes about 150 minutes to warm up to room temperature.

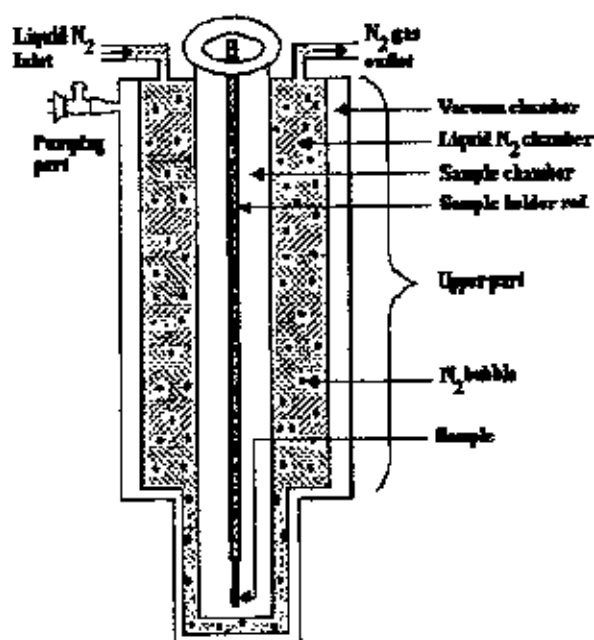


Figure 3.4: Schematic diagram of the liquid nitrogen cryostat.

3.5.2 Description of electromagnet

To study magneto-transport properties of manganese perovskites the electromagnet used is shown in Figure 3.5. Materials play an important role for designing an electromagnet. Normally soft iron with a very low coercive field and low hysteresis is used for the magnet pole pieces. Commercial mild steel bar is used for the body of the electromagnet and soft iron cylindrical rod for pole pieces, which are available in the local market (Dhaka, Bangladesh).

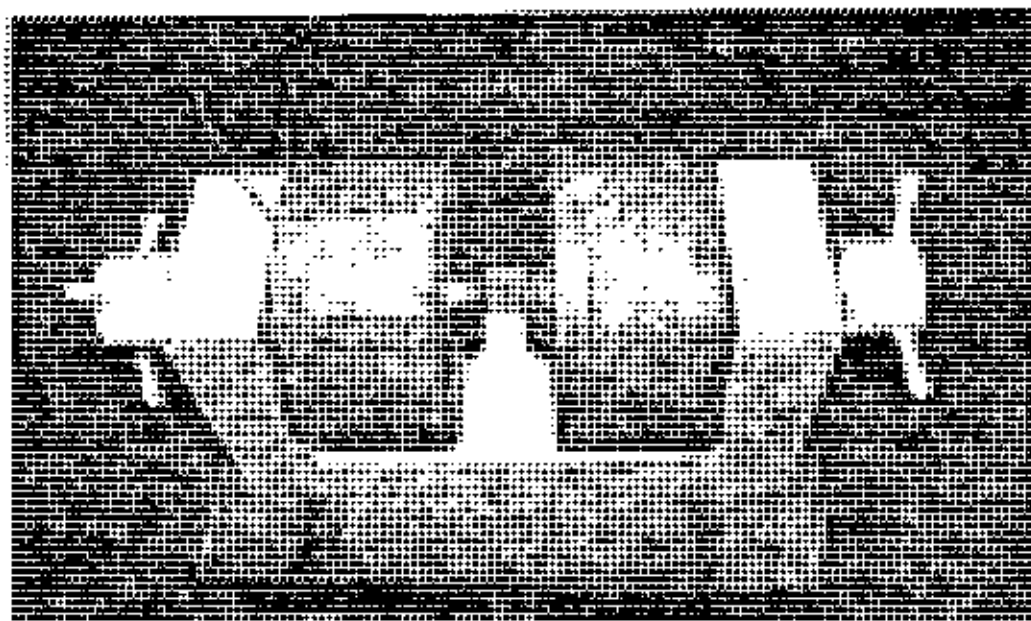


Figure 3.5: Photograph of the electromagnet.

The major parts of the electromagnets are base, pole piece holder, pole pieces and coils. Base of the electromagnet is made up of a parallelepiped shaped mild steel bar of dimension $36\text{ cm} \times 19\text{ cm} \times 8\text{ cm}$. Pole piece holder of the electromagnet is also made from commercial mild steel bar. Two pole piece holders are attached to both side of the base with L type bolt. Each pole piece holder is a parallelepiped of dimension $32\text{ cm} \times 19\text{ cm} \times 8\text{ cm}$. Pole pieces (cylindrical soft iron of final diameter 9.2 cm) are attached in these holders in such a way so that we can vary the pole gap. The Pole gap may vary from $0\text{-}10\text{ cm}$. As the lower part of our cryostat has outer dimension 3.8 cm , pole gap of this size will be suitable for the magnet operation.

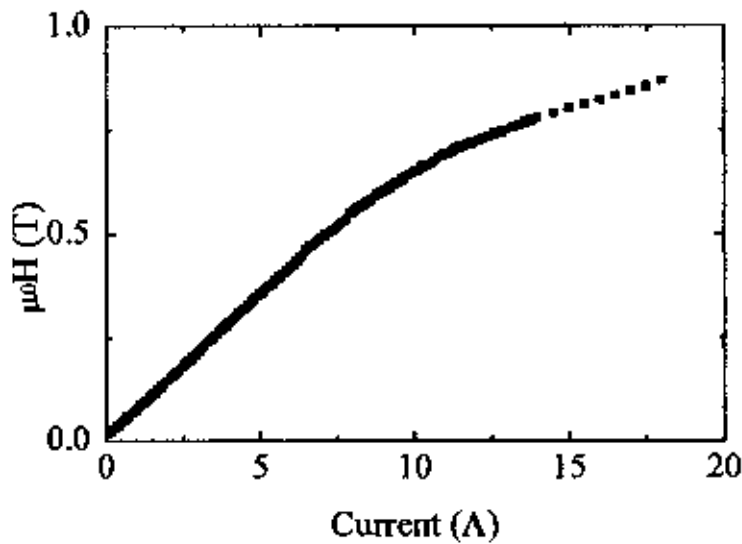


Figure 3.6: Calibration curve of the electromagnet.

Two induction coils for two pole-pieces have been made with insulated copper wire of No. S. W. G 14. The length of each of the coils is 12 cm. The number of turns in each layer of the coil is 58 and total number of layers is 44. So the total number of turns is 2552. The resistance of each coil is about 8 Ω . The weight of each coil is about 40 Kg. Two coils are set in the pole pieces of the electromagnet. They are connected in parallel combination with the dc power supply. Calibration curve of the electromagnet is given in Figure 3.6.

3.5.3 Description of the sample rod

A sample rod is used for four-point resistance measurement. This is a hollow stainless steel tube. The upper part is connected with multi-pin connectors and lower part has a copper sample holder as shown in figure. The sample rod is connected with the cryostat by a union socket. A schematic diagram of the sample rod is shown in figure 3.7. This sample probe is used for four point resistance measurements. The temperature of the sample was measured using a thermocouple.

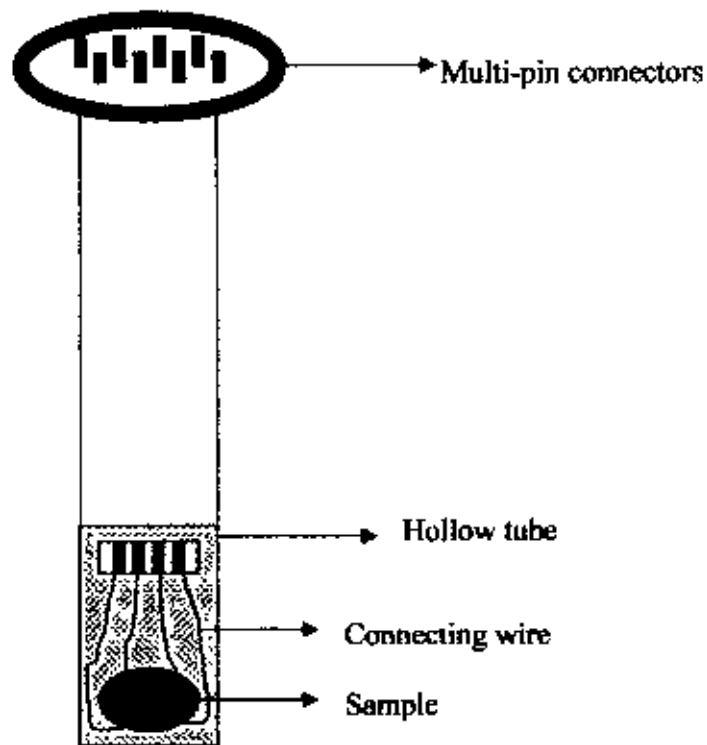


Figure 3.7: Schematic diagram of the sample rod.

3.5.4. Magnetoresistance measurement setup

Magnetoresistance measurements were carried out using the homely made cryostat and an electromagnet. Figure 3.8 shows the schematic diagram of the magnetoresistance measurement.

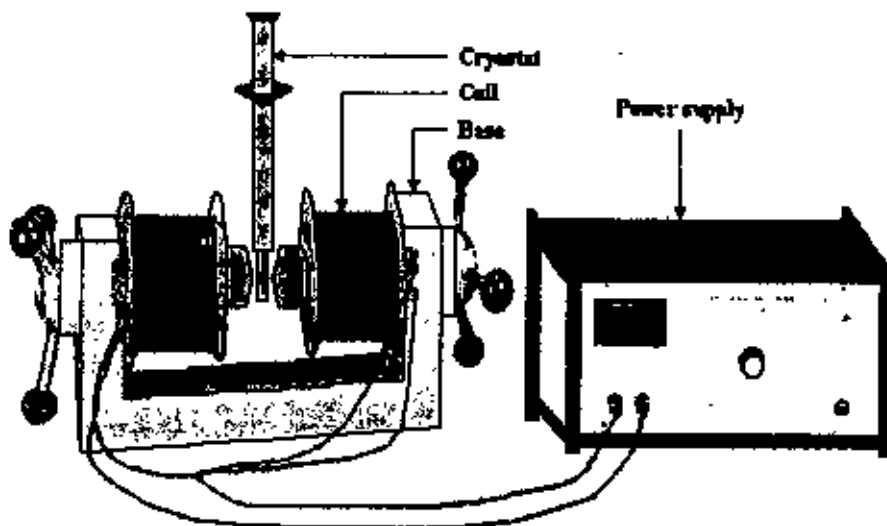


Figure 3.8: Schematic diagram of magnet and cryostat assembly for magnetoresistance measurements.

The standard four point technique was used for resistance measurements. All samples for test are mounted on a probe and inserted in the sample well of the cryostat. The temperature of the sample is measured with a thermocouple placed close to the sample. A micro voltmeter was placed with the thermocouple to measure the voltage related to the temperature. The sample current is sourced with a constant current source and voltage drop is measure with micro voltmeter. For magnetoresistance measurements, the electromagnet is powered with a power supply. The system is capable of creating a field up to 0.86T for a current of 18 A.

References

- 104313
- [1] van der Pauw L.J., "A method of measuring specific resistivity and Hall effects of discs of arbitrary shape", Philips research reports, **13**, 1 (1958).
 - [2] van der Pauw L.J., "A method of measuring specific resistivity and Hall coefficient on lamellae of arbitrary shape", Philips technical review, **20**, 220 (1958).

Chapter-4

Results and Discussion

The transport properties of the polycrystalline bulk samples of $(La_{1.6}Dy_{0.2}Sr_{1.2})(Mn_{2-x}Fe_x/Ni_x)O_7$ (with $x=0.0, 0.1, 0.2$) sintered at temperature $1100^{\circ}C$ and constant hydrostatic pressure were studied. The results of DC electrical measurements including resistivity, phase transitions and magnetoresistive properties were measured from room temperature (RT) down to liquid nitrogen temperature (LN_2T). Magnetoresistance (MR) measurements were carried out and the MR behaviour was discussed as a function of magnetic field both at room temperature and at liquid nitrogen temperature. Activation energies for these polycrystalline samples were also calculated in this experiment.

4.1 X-ray diffraction analysis

X-ray diffraction analysis was performed on the investigated polycrystalline samples to examine phase purity and homogeneity. Figure 4.1 shows the X-ray diffraction pattern for various sample $(La_{1.6}Dy_{0.2}Sr_{1.2})(Mn_{2-x}Fe_x/Ni_x)O_7$ (with $x=0.0, 0.1, 0.2$). The X-ray diffraction was recorded with a powder diffractometer using the MoK α radiation ($\lambda=0.710689 \text{ \AA}$). For the structure determination, diffraction patterns were recorded in the 2θ range from 10° to 70° . Table 4.1 shows the comparative peak position (in angle) observed for the samples. The peaks in an X-ray diffraction pattern are directly related to the atomic distance. From the peaks in an X-ray diffraction pattern the inter-planer distance d_{hkl} is measured using Bragg's law

$$d_{hkl} \sin\theta = n\lambda \dots\dots\dots(4.1)$$

where λ is the wavelength of the X-ray and θ is the scattering angle of the diffraction peak. From the X-ray diffraction patterns it have seen that all the samples showed the identical peak positions which confirmed the single phase with no significant trace of impurity in chemical composition of the samples.

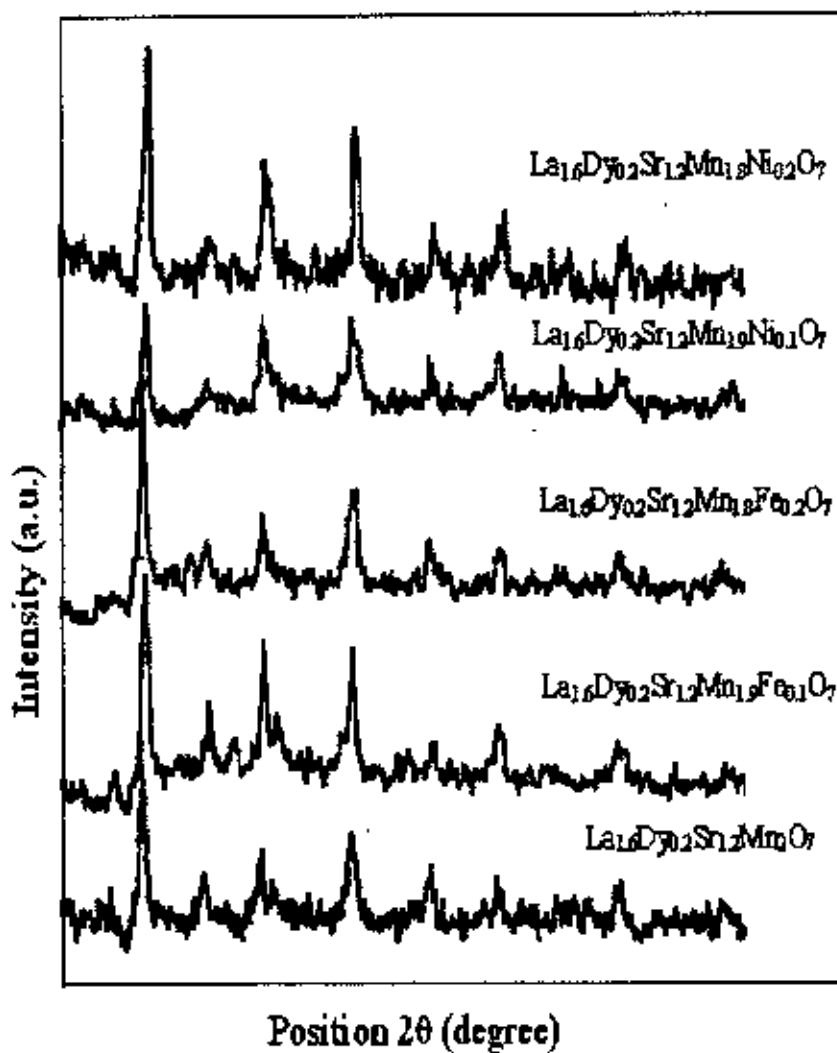


Figure 4.1: X-ray diffraction patterns of polycrystalline bulk samples.

Table 4.1: X-ray diffraction peak positions for various polycrystalline samples

Sample Compositions	X-ray diffraction peak position 2θ (degree)						
	1 st	2 nd	3 rd	4 th	5 th	6 th	7 th
$(La_{1-x}Dy_{0.2}Sr_{1.2})Mn_2O_7$	14.4	17.60	20.72	25.56	29.68	33.28	39.80
$(La_{1-x}Dy_{0.2}Sr_{1.2})(Mn_{1.9}Fe_{0.1})O_7$	14.64	18.00	20.88	25.6	29.96	33.44	39.80
$(La_{1-x}Dy_{0.2}Sr_{1.2})(Mn_{1.8}Fe_{0.2})O_7$	14.48	18.00	20.80	25.92	29.80	33.60	39.96
$(La_{1-x}Dy_{0.2}Sr_{1.2})(Mn_{1.9}Ni_{0.1})O_7$	14.60	17.96	20.80	25.60	29.76	33.44	39.68
$(La_{1-x}Dy_{0.2}Sr_{1.2})(Mn_{1.8}Ni_{0.2})O_7$	14.72	18.00	20.88	25.68	29.80	33.68	39.80

4.2 DC electrical resistivity

The normalized DC electrical resistivity for various $(La_{1-x}Dy_{0.2}Sr_{1.2})(Mn_{2-x}Ni_x/Fe_x)O_7$ polycrystalline samples prepared for doping levels $x=0.0, 0.1, 0.2$ and sintered at temperature 1100°C for 24 hours in air were measured as a function of temperature from room temperature (300K) down to liquid nitrogen temperature (78K) by standard four probe method. The temperature dependence of normalized resistivity ρ/ρ_0 at zero applied magnetic field for various polycrystalline samples and corresponding behaviour in presence of 0.7T applied magnetic field was investigated. The applied magnetic field was perpendicular to the current flow in the sample.

The temperature dependence of normalized resistivity ρ/ρ_0 of the double layered perovskite manganites $(La_{1-x}Dy_{0.2}Sr_{1.2})(Mn_{2-x}Fe_x)O_7$ with different concentrations $x=0.0, 0.1, 0.2$ at zero magnetic field and at the presence of 0.7T magnetic field are shown in figure 4.2 and 4.3.

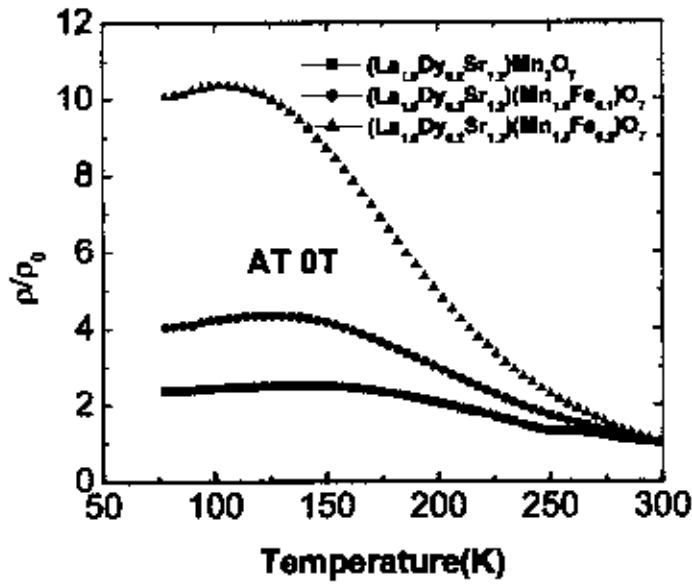


Figure 4.2: Normalized resistivity as a function of temperature for $(La_{1.6}Dy_{0.2}Sr_{1.2})(Mn_{2-x}Fe_x)O_7$ with $x=0.0, 0.1$ and 0.2 at $0T$ magnetic field.

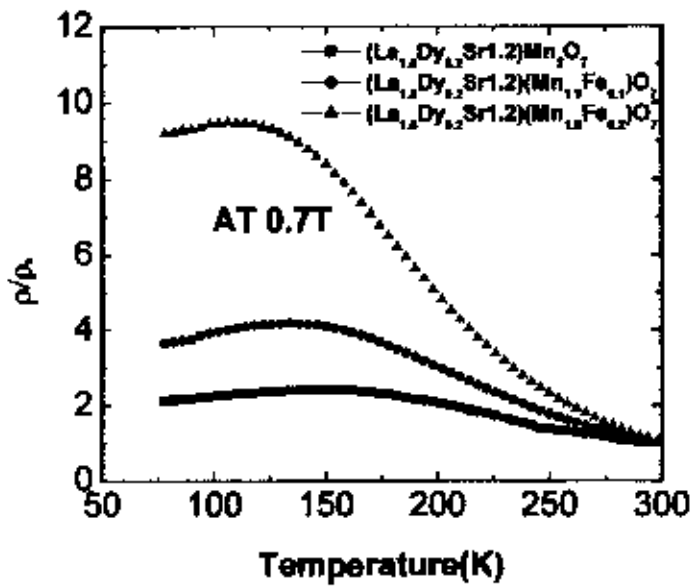


Figure 4.3: Normalized resistivity as a function of temperature for $(La_{1.6}Dy_{0.2}Sr_{1.2})(Mn_{2-x}Fe_x)O_7$ with $x=0.0, 0.1$ and 0.2 at $0.7T$ magnetic field

From figures 4.2 and 4.3 it is observed that for all samples resistivity first increase with the decrease in temperature, and show a metal- insulator transition with a peak in the electrical resistivity ρ , at a temperature T_p . For $T > T_p$ resistivity decreases with the increase of temperature. For insulating behaviour it is noted that $d\rho/dT < 0$ for $T > T_p$. But for $T < T_p$ the sample showed metallic character with $d\rho/dT > 0$. Concentrating on the behaviour of temperature dependence of resistivity it is observed that T_p decreases but resistivity increases with the external magnetic field which is shown in the table 4.2.

Dorr *et.al.*[1] observed a metal insulator transition near a ferromagnetic ordering temperature which is associated with a large negative magnetoresistance for the double layered polycrystalline bulk samples $\text{La}_{2-2x}\text{Sr}_{1+2x}\text{Mn}_2\text{O}_7$ with doping levels of $x = 0.3$ and 0.5 .

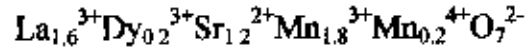
Asano *et.al.*[2] reported the results on the MR properties of epitaxial film and polycrystalline bulk samples of double layered perovskite $\text{La}_{2-2x}\text{Ca}_{1+2x}\text{Mn}_2\text{O}_7$ ($x = 0.3$). Large MR effect at temperature around the metal –insulator transition was observed for both samples.

Basith *et.al.* [3] have measured magnetoresistive properties of Gd doped polycrystalline samples of Ruddlesden-Popper series $(\text{La}_{1-x}\text{Sr}_x)_{n+1}\text{Mn}_n\text{O}_{3n+1}$ ($n=2$), sintered at temperature 1100°C for 24 hrs in air, from room temperature down to liquid nitrogen temperature using standard four-probe technique. In the measurements of Dorr *et.al.*[1], Asano *et.al.*[2], and Basith *et.al.* [3], the exhibited electrical and magnetic transport properties in this double-layered manganites were described by double-exchange mechanism.

The layered perovskite manganites $(\text{La}_{1-x}\text{Dy}_x)_{n+1}\text{Mn}_n\text{O}_{3n+1}$ the transport behavior the simultaneous ferromagnetic and metal- insulator transition can be understood within the framework of double-exchange model proposed by Zener [4]

The parent material $(\text{LaDy})_2\text{SrMn}_2\text{O}_7$ is a charge transfer insulator. When divalent Sr ions are substituted in place of trivalent La to produce $\text{La}_{1.6}\text{Dy}_{0.2}\text{Sr}_{1.2}\text{Mn}_2\text{O}_7$, charge

neutrality is disturbed. To keep the material neutral a part of Mn valency changes from Mn^{3+} to Mn^{4+} in the following manner



In the $La_2SrMn_2O_7$ in which only Mn^{3+} exists. The presence of Mn^{4+} , due to the doping, enables the e_g electron of Mn^{3+} ion to hop to the neighboring Mn^{4+} ion via DE which ultimately mediates ferromagnetism and conduction.

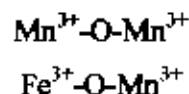
In the last few years, there have been considerable reports on the effects of Mn-site substitution by elements such as Fe, Co, Ni, Al, Cr etc. Kasper et.al.[5] showed that with Fe doping at the Mn site caused to decrease of metal-insulator transition temperature.

Xianyu et.al.[6] studied Fe doped $La_{1-x}Sr_xMnO_3$ system. They also reported with increase of x, metal-insulator transition temperature increases, becomes maximum at $x=0.4$ and then decreases.

In the present investigation the normalized resistivity increases with increasing Fe content and the transition temperature is decreased. When trivalent Fe ions are substituted in place of trivalent Mn to produce $(La_{1.6}Dy_{0.2}Sr_{1.2})(Mn_{2-x}Fe_x)O_7$ a part of Mn valence changes from Mn^{3+} to Fe^{3+} in the following manner



When Fe is substituted in place of Mn, the disorder introduced by the Fe doping combined with the replacement of some of the Mn-O-Mn bonds by Mn-O-Fe bonds:



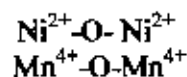
This observation can be explained considering the super-exchange interactions in the orbital disordered state the exchange interaction $Mn^{3+}-O-Mn^{3+}$ is positive, at the same time the exchange $Fe^{3+}-O-Mn^{3+}$ is negative[7], so the substitution of Mn^{3+} with Fe^{3+} lead to decrease of transition temperature.

Figures 4.4 and 4.5 show the normalized resistivity as a function of temperature for double layered perovskite samples $(La_{1-x}Dy_xSr_{1.2})(Mn_{2-x}Ni_x)O_7$ with $x= 0.0, 0.1$ and 0.2 at zero magnetic field and at the presence of $0.7T$ magnetic field respectively. In those figure all the samples showed a metal-insulator transition with a peak in the electrical resistivity around M-I transition temperature, T_p like the previous double layered samples. Here the increases of Ni doping concentration the resistivity increases but M-I transition temperature, T_p decreases,

When Mn is substituted by Ni, the combination of Ni^{2+} and Mn^{4+} has been observed to be favourable. When divalent Ni ions are substituted in place of trivalent Mn to produce $(La_{1-x}Dy_xSr_{1.2})(Mn_{2-x}Ni_x)O_7$ charge neutrality is disturbed. To keep the material neutral a part of Mn valence changes from Mn^{4+} to Ni^{2+} in the following manner



With the doping some of the $Ni^{2+}-O-Ni^{2+}$ bonds and also some of the $Mn^{4+}-O-Mn^{4+}$ bonds, which are coupled antiferromagnetically with the nearest neighbours appears. When Ni is substituted in place of Mn, the disorder introduced by the Ni doping combined with the replacement of some of the Mn-O-Mn bonds by Mn-O-Ni bonds:



Substitution of Mn by Ni destroys the long range ferromagnetic order and it has been observed that Ni doping at Mn site weakens ferromagnetism in the magnetic system. [8]. Thus with the increases of Ni concentration resistivity increases and the metal-insulator transition temperature decreases.

Sudipta *et. al.*[9] observed with Ni doped $\text{La}_{1.7}\text{Pb}_{0.3}\text{Mn}_{1-x}\text{Ni}_x\text{O}_3$ ($x=0-0.5$) system exhibits decrease of resistivity and increase of metal-insulator transition temperature.

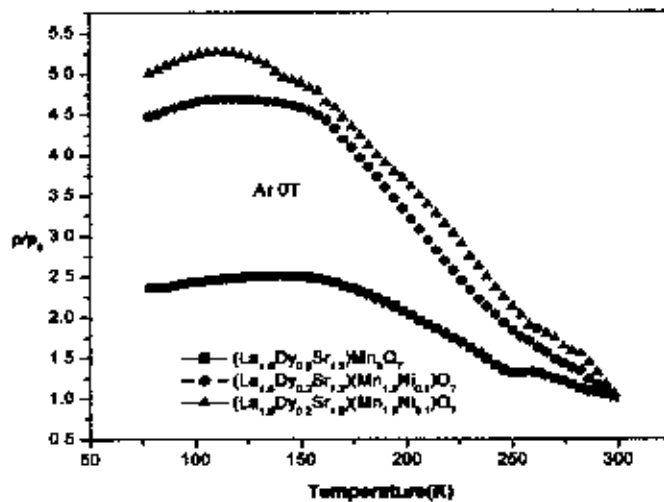


Figure 4.4: Normalized resistivity as a function of temperature for $(\text{La}_{1.6}\text{Dy}_{0.2}\text{Sr}_{1.2})(\text{Mn}_{2-x}\text{Ni}_x)\text{O}_7$ with $x=0.0, 0.1$ and 0.2 at 0T magnetic field.

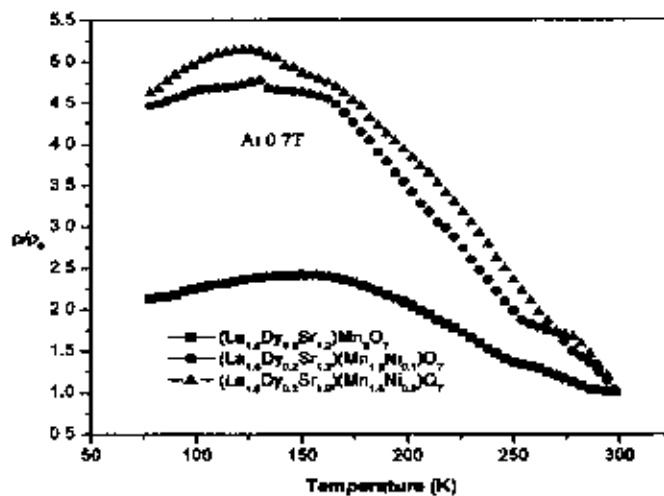


Figure 4.5: Normalized resistivity as a function of temperature for $(\text{La}_{1.6}\text{Dy}_{0.2}\text{Sr}_{1.2})(\text{Mn}_{2-x}\text{Ni}_x)\text{O}_7$ with $x=0.0, 0.1$ and 0.2 at 0.7T magnetic field.

Table 4.2: Transition temperatures, T_p and normalized resistivity at the magnetic field 0T and 0.7T

Sample Composition	T_p at 0T	ρ/ρ_0 at 0T	T_p at 0.7T	ρ/ρ_0 at 0.7T
$(La_{1.6}Dy_{0.2}Sr_{1.2})Mn_2O_7$	135	2.51	150	2.42
$(La_{1.6}Dy_{0.2}Sr_{1.2})(Mn_{1.9}Fe_{0.1})O_7$	125	4.34	134	4.19
$(La_{1.6}Dy_{0.2}Sr_{1.2})(Mn_{1.2}Fe_{0.2})O_7$	112	10.30	121	9.49
$(La_{1.6}Dy_{0.2}Sr_{1.2})(Mn_{1.9}Ni_{0.1})O_7$	119	4.68	131	4.81
$(La_{1.6}Dy_{0.2}Sr_{1.2})(Mn_{1.2}Ni_{0.2})O_7$	103	5.24	117	5.68

In this investigation it is also observed that in the presence of 0.7T magnetic field the value resistivity decrease to lower values but M-I transition temperature, T_p shifts towards the higher temperature region. Fe and Ni substitution may also favor the charge carrier delocalization induced by the magnetic field, which suppresses the resistivity. The application of magnetic field enhances magnetic spin order and due to this ordering, the ferromagnetic metallic state suppresses the paramagnetic insulating state, which ultimately shift T_p towards the higher temperature region.

4.3 Magnetoresistance of various polycrystalline samples

Magnetoresistance (MR) refers to the relative change in the electrical resistivity of a material on the application of an external magnetic field. MR is generally defined as

$$MR\% = - \{p(H) - \rho(0)\} / p(0) \times 100$$

Where $\rho(0)$ is the resistivity obtained without magnetic field and $\rho(H)$ is the resistivity measured under magnetic field 0.7T. The magnetoresistance as a function of magnetic field for samples $(La_{1.6}Dy_{0.2}Sr_{1.2})(Mn_{2-x}Fe_x/Ni_x)O_7$ ($x=0.0, 0.1, 0.2$) were calculated at room temperature (300K) and at liquid nitrogen temperature (78K). Typical MR curves as function of magnetic field obtained at room temperature are shown in figure 4.6. Room

temperature MR is found to be very low with a maximum value 1.69% with in the range of 0 to 860 mT and was almost linear with field.

A large value of MR is observed at 78K in the presence of low applied magnetic field. Hence it is clear that the degrees of spin polarization in these manganites are temperature dependent and increases with decreasing temperature just like $R_{1-x}A_xMnO_3$ manganites. At low temperature (78K) the strong linear field dependence of MR exists for a field of upto H^* as shown in figure 4.7. The magnetic field H^* designates the boundary of the two slopes. Beyond H^* the magnetoresistance is a weak function of the applied magnetic field. In this work about 27% of the MR is observed at $H^* = 327$ mT, for $(La_{1-x}Dy_{0.2}Sr_{1.2})(Mn_{1-x}Ni_{0.2})O_7$. In these cases, applied magnetic field was perpendicular to the sample. The value of MR the corresponding H^* for each sample at the liquid nitrogen temperature (78K) are shown in table 4.4. It is observed that with the increase of Fe and Ni doping the percentage of MR is increased.

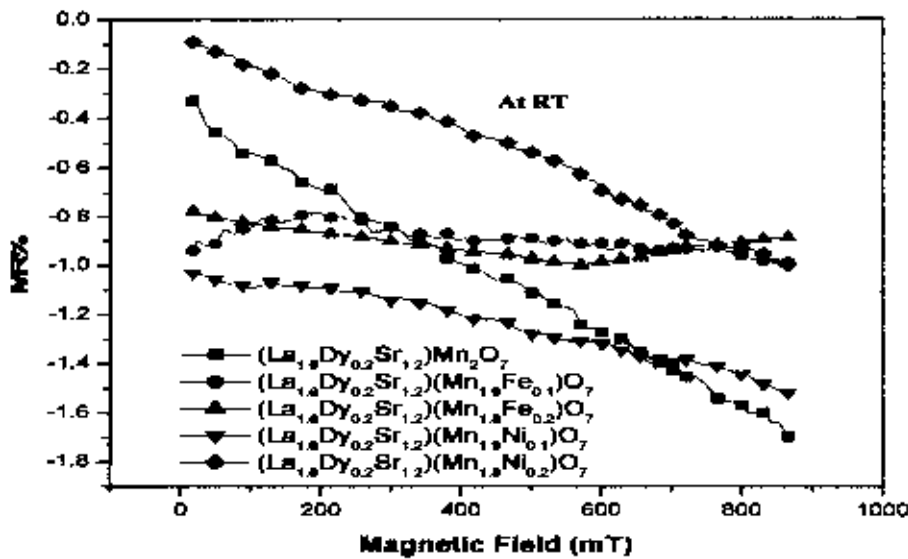


Figure 4.6: Magnetoresistance (MR) as a function of magnetic field at room temperature for various polycrystalline samples

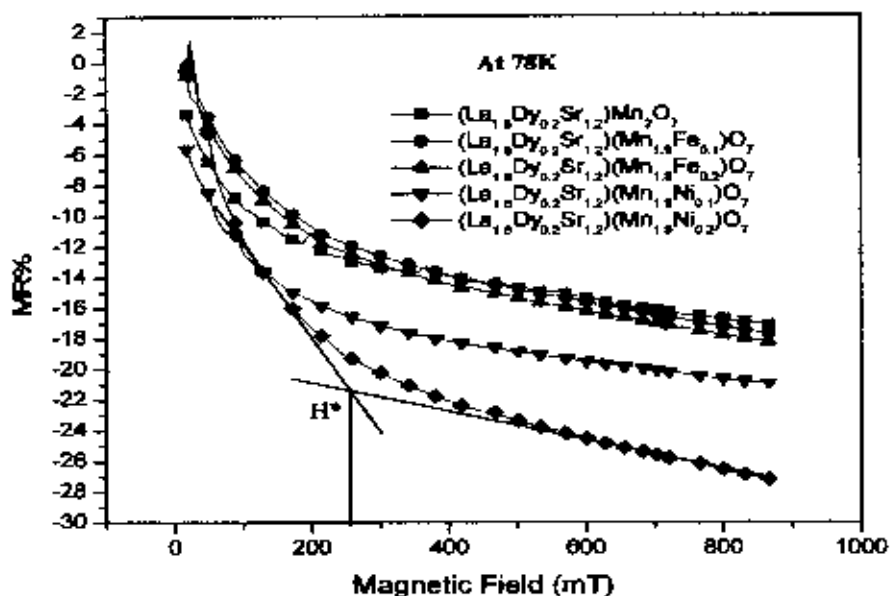


figure 4.7: Magnetoresistance (*MR*) as a function of magnetic field at 78K temperature for various polycrystalline samples $(\text{La}_{1-x}\text{Dy}_{0.2}\text{Sr}_{1.2})(\text{Mn}_{2-x}\text{Fe}_x)\text{O}_7$ and $(\text{La}_{1-x}\text{Dy}_{0.2}\text{Sr}_{1.2})(\text{Mn}_{2-x}\text{Ni}_x)\text{O}_7$ with $x=0.0, 0.1$ and 0.2

Table 4.4: Table for H^* , MR at H^* and Maximum MR at 78K for various polycrystalline materials

Sample Composition	Maximum H(mT)	H^* (mT)	MR%	maximum MR%
$(\text{La}_{1-x}\text{Dy}_{0.2}\text{Sr}_{1.2})\text{Mn}_2\text{O}_7$		227	12.42	17.08
$(\text{La}_{1-x}\text{Dy}_{0.2}\text{Sr}_{1.2})(\text{Mn}_{1-x}\text{Fe}_{0.1})\text{O}_7$		293	12.57	18.22
$(\text{La}_{1-x}\text{Dy}_{0.2}\text{Sr}_{1.2})(\text{Mn}_{1-x}\text{Fe}_{0.2})\text{O}_7$	860	312	13.37	17.67
$(\text{La}_{1-x}\text{Dy}_{0.2}\text{Sr}_{1.2})(\text{Mn}_{1-x}\text{Ni}_{0.1})\text{O}_7$		300	17.14	20.94
$(\text{La}_{1-x}\text{Dy}_{0.2}\text{Sr}_{1.2})(\text{Mn}_{1-x}\text{Ni}_{0.2})\text{O}_7$		327	20.81	27.20

The two slopes MR at low temperature were explained by Akther Hossain et. al [10] in following grain and grain boundary model. According this model, the materials are subdivided into domains and low applied field is quite sufficient to align the domain spins and thus a sharp decrease in MR is observed. But to align the misaligned spins at the domain boundary region requires much larger field leading to weak field dependence. At $T \ll T_c$ the material is in the ferromagnetic regime. In the absence of the field the magnetization of the grain of the polycrystalline material will be like that in fig. (a). The

individual spins at the grain boundary region are randomly oriented. In the absence of the field, a carrier will suffer scattering from the unaligned magnetic domain, as well as disordered spin at the grain boundary region. By applying a low magnetic field, the magnetization of each grain starts to align towards the direction of the external magnetic field as fig. (b). However, a large magnetic field is required to align the spins of the grain boundaries.

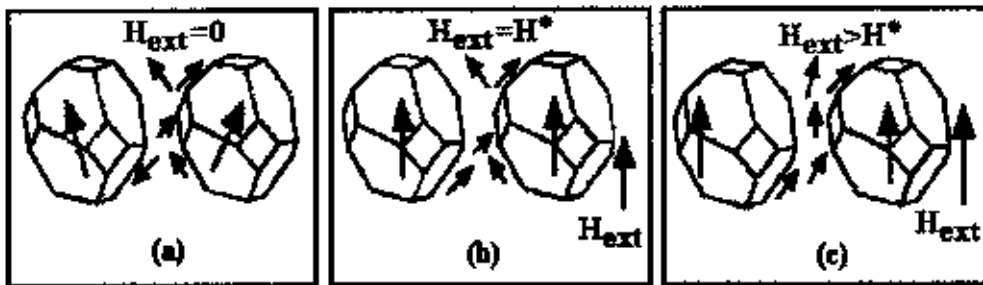


Figure 4.8: Schematic illustration of domain-boundary transport in a polycrystalline mixed-valence manganite

The other possible explanation of low field MR effect in these manganites is that when traveling across the grain boundary, conduction electrons may be subjected to a strong spin-dependent scattering. This scattering is reduced if a low external magnetic field can align the magnetizations of the neighbouring grains.

4.4: Activation energy

The insulating-like behaviour of resistivity at temperature above T_p generally can be explained by activation energy for the samples which is calculated from the slopes of straight lines using the relation

$$\rho = \rho_0 \exp(E_0 / K_B T) \dots\dots\dots (4.2)$$

where, E_0 is the activation energy and K_B is the Boltzmann constant. In figure 4.9 $\ln \rho / \rho_0$ is plotted against $1/T$ for various $(La_{1-x}Dy_{0.2}Sr_{1.2})(Mn_{2-x}Fe_x/Ni_x)O_7$ ($x=0.0, 0.1, 0.2$) samples at sintering temperature $1100^\circ C$ and applied magnetic field $0 T$ and $0.7 T$. The

temperature region is considered from transition temperature to room temperature for the respective polycrystalline samples.

Activation energy is then given by

$$E_0 = [\ln(\rho/\rho_0)] K_B$$

$$= \text{slope} \times K_B \dots\dots\dots (4.3)$$

The corresponding activation energies for different samples are given in table 4.5.

Table 4.5: Activation energy (meV) of the polycrystalline samples

Sample Composition	Activation energy (meV) 0T	Activation energy (meV) 0.7T
(La _{1.6} Dy _{0.2} Sr _{1.2})Mn ₂ O ₇	5.61	5.53
(La _{1.6} Dy _{0.2} Sr _{1.2})(Mn _{1.9} Fe _{0.1})O ₇	8.04	7.99
(La _{1.6} Dy _{0.2} Sr _{1.2})(Mn _{1.8} Fe _{0.2})O ₇	12.52	12.35
(La _{1.6} Dy _{0.2} Sr _{1.2})(Mn _{1.9} Ni _{0.1})O ₇	7.29	6.44
(La _{1.6} Dy _{0.2} Sr _{1.2})(Mn _{1.8} Ni _{0.2})O ₇	7.97	7.93

Figure 4.9 shows that the activation energy with applied 0.7 T magnetic field is smaller than that of the energy without magnetic field .All the samples show very good linear behavior in the $\ln(\rho/\rho_0)$ vs $1/T$ curve which suggest that conduction occurs through a thermally activated process. [11]

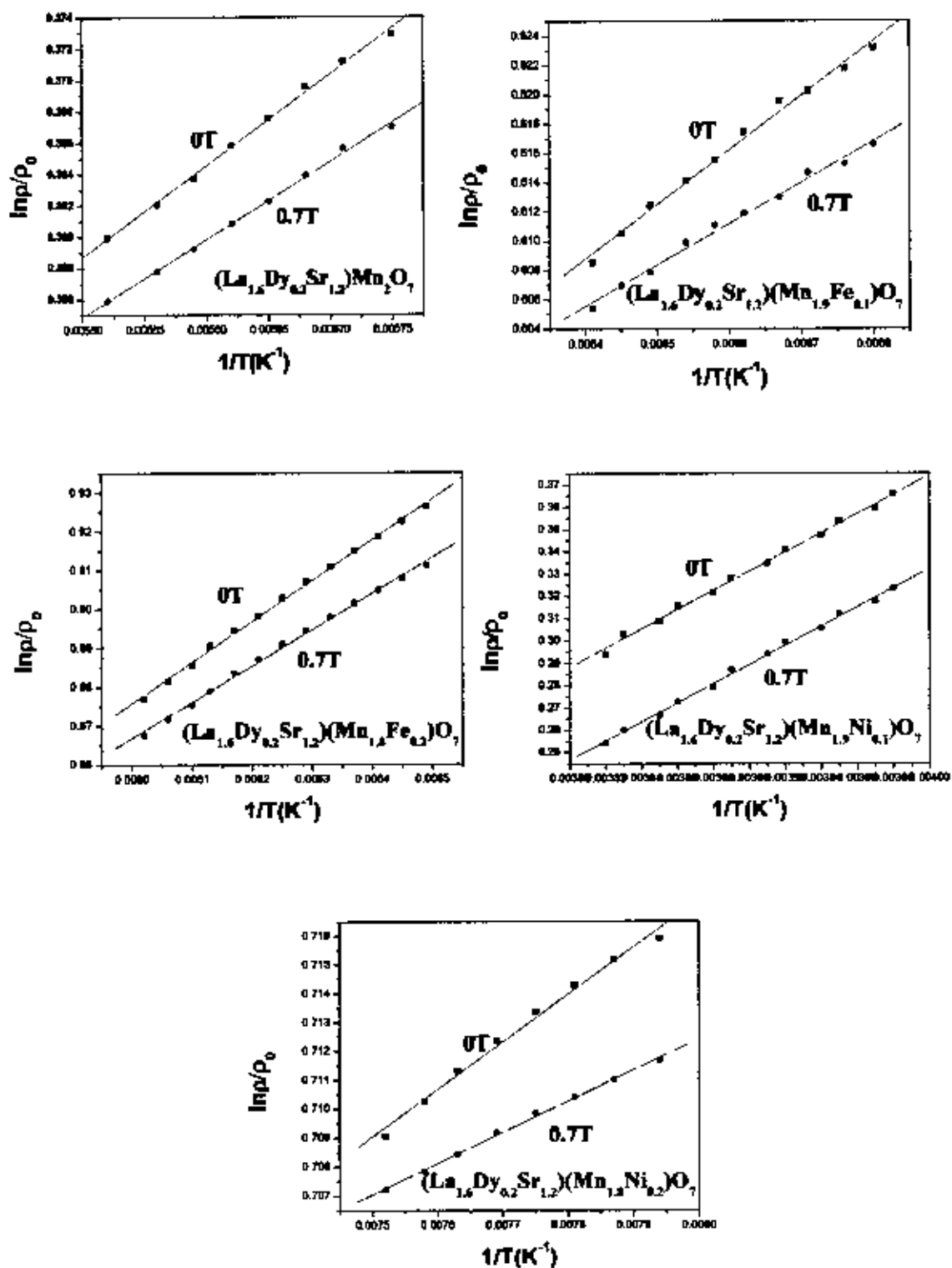


Figure 4.9: $\ln(\rho/\rho_0)$ is plotted against $1/T$ for various polycrystalline samples

Reference

- [1] Dorr, K, Muller.K.H., Ruck.K., Krabbes.G., and Schultz. L., "Magnetoresistance of polycrystalline layered manganites $\text{La}_{2-2x}\text{Sr}_{1+2x}\text{Mn}_2\text{O}_7$ ". J.Appl.Phys.85 No.8, (1999)
- [2] Asano.H., Hayakawa. J., and Matsue. M., "Magnetoresistance in thin film and bulk of layered perovskite $\text{La}_{2-2x}\text{Ca}_{1+2x}\text{Mn}_2\text{O}_7$ ". Appl.Phys.Rev.B 57, 72 (1997)
- [3] Basith, M.A. and Huq, M., "Magnetoresistance properties of Gd doped Lanthanum strontium Manganites", Journal of Ultra Chemistry, Vol. 1, No-229-36(2005)
- [4] Zener, C., "Interaction between d shells in the transition metals (ii) Ferromagnetic compounds of manganese with perovskite structure." Phys.Rev. 82,403 (1961)
- [5] Kasper N. V., Journal of Magnetism and Magnetic Materials, 222,28-32,(2000)
- [6] Xianyu Wen-xu, Li Bao-he, Qian Zheng-nam, Jin Han-mim "Effect of Fe doping in $\text{La}_{1-x}\text{Sr}_x\text{MnO}_3$ ", Journal of applied Physics, 86,5164-5178(1999)
- [7] Goodenough J.B., "Magnetism and the Chemical Bond," Interscience, New York, (1963)
- [8] Sanchez , Phy Rev B, 65 (2002), 144409
- [9] Sudipta Pal, Esa Bose, Chaudhuri B.K., Yang H.D., Neeleshwar S., Chen, Y. Y. "Effect of Ni doping in rare-earth manganite $\text{La}_{0.7}\text{Pb}_{0.3}\text{Mn}_{1-x}\text{Ni}_x\text{O}_3$ ($x=0.0-0.5$)", Journal of magnetism and magnetic materials, 293, 872 (2005).
- [10] Akther Hossain A K M, Cohen L F, Berenov A, Macmanus Driscoll J L, "Highly sensitive low temperature Low field colossal magnetoresistance in screen printed $\text{La}_{0.63}\text{Y}_{0.07}\text{Ca}_{0.30}\text{MnO}_3$ thick films" Materials Science & Engineering B, 83(1-3), 79-83 (2001).
- [11] Barman, A., Ghosh, M., Biswas, S., De, S.K., and Chatterjee, S., "Charge ordered state and giant Magnetoresistance in $\text{Pr}_{0.7}\text{R}_{0.1}\text{Ca}_{0.2}\text{MnO}_3$ (R=Y,Dy,Gd,Sm and Nd)." J.Phys.Condens.Matt.10, L199 (1998)

Chapter-5

Conclusions

Magnetoresistive properties of $(La_{1-x}Dy_xSr_{1-2})(Mn_{2-x}Fe_x/Ni_x)O_7$ bulk polycrystalline samples prepared for doping levels ($x = 0.0, 0.1, 0.2$) and sintered at temperature 1100°C for 24 hours in air were investigated from room temperature down to liquid nitrogen temperature using standard four-probe technique at an applied magnetic field 0T and 0.7T. The structure and phase purity of the samples were checked by powder X-ray diffraction (XRD) using MoK_α radiation by X-ray Diffractometer. The XRD patterns have confirmed the homogenous and single phase perovskite structure of all the samples with no significant trace of impurity.

In the present investigation all the samples exhibit metal-insulator (M-I) transition when the temperature is decreased from room temperature down to liquid nitrogen temperature. This M-I transition has been interpreted within the framework of Zener double exchange mechanism.

Although the magnetic moment of Fe ($5\mu_B$) is higher than that of Mn^{3+} ($4\mu_B$), one can see that the normalized resistivity increases with increasing Fe content and the transition temperature is decreased. This observation can be explained considering the super-exchange interactions in the orbital disordered state the exchange interaction $\text{Mn}^{3+}\text{-O-Mn}^{3+}$ is positive, at the same time the exchange $\text{Fe}^{3+}\text{-O-Mn}^{3+}$ is negative, so the substitution of Mn^{3+} with Fe^{3+} lead to decrease of transition temperature. Substitution of Mn by Ni destroy the long range ferromagnetic order and it has been observed that Ni doping at Mn site weakens ferromagnetism in the magnetic system. Thus with the increases of Ni concentration resistivity increases and the metal-insulator transition temperature decreases. But this substitution of Ni is Tp and resistivity is smaller than Fe.

The resistivity vs temperature graphs with applied field in the same samples show similar behaviour except the enhancement of M-I transition temperature by few Kelvin. This

would be due to the suppression of spin fluctuations with the applied field in the paramagnetic region.

MR behaviour at room temperature for all samples found very low and is almost linear with field. At 78 K, a sharp increase of magnetoresistance was observed at low magnetic fields followed by a weak and linear dependence at high fields. The observed low temperature MR in these manganites can be attributed to grain and grain boundary effects. The plot of $\ln(\rho/\rho_0)$ vs T^{-1} suggests that conduction occurred through a thermally activated process above the transition temperature.

